Article

Chitosan/Perlite System as a Microbial Carrier in Anaerobic Digestion of Food Waste: Characteristics and Impact of the Additive Materials

Agnieszka A. Pilarska *, Anna Marzec-Grządziel, Małgorzata Makowska, Alicja Kolasa-Więcek, Ranjitha Jambulingam, Tomasz Kałuża, Krzysztof Pilarski

Posted Date: 12 June 2024

doi: 10.20944/preprints202406.0813.v1

Keywords: chitosan/perlite system; physicochemical properties; impact of additives; anaerobic digestion; FTIR spectroscopy; NGS analysis

 doi:10.20944/preprints202406.0813.v1

Article

Chitosan/Perlite System as a Microbial Carrier in Anaerobic Digestion of Food Waste: Characteristics and Impact of the Additive Materials

Agnieszka A. Pilarska [1,*], Anna Marzec-Grządziel [2], Małgorzata Makowska [1], Alicja Kolasa-Więcek [3], Ranjitha Jambulingam [4], Tomasz Kałuża [1] and Krzysztof Pilarski [5]

[1] Department of Hydraulic and Sanitary Engineering, Poznań University of Life Sciences, Piątkowska 94A, 60-649 Poznań, Poland; malgorzata.makowska@up.poznan.pl (M.M.)
[2] Department of Agriculture Microbiology, Institute of Soil Science and Plant Cultivation – State Research Institute, Czartoryskich 8, 24-100 Puławy, Poland; agrzadziel@iung.pulawy.pl (A.M.-G.)
[3] Institute of Environmental Engineering and Biotechnology, Faculty of Natural Sciences and Technology, University Opole, Kominka 6, 46-020 Opole, Poland; akolasa@uni.opole.pl (A.K-W.)
[4] CO_2 Research and Green Technologies Centre, Vellore Institute of Technology, Vellore, Tamil Nadu, India; ranjitha.j@vit.ac.in (R.J.)
[5] Department of Biosystems Engineering, Poznań University of Life Sciences, Wojska Polskiego 50, 60-627 Poznań, Poland; pilarski@up.poznan.pl (K.P.)
* Correspondence: Tel.: +48 61 846 65 93. E-mail address: pilarska@up.poznan.pl (A.A. Pilarska.).

Abstract: The article aims to present the results of research on anaerobic digestion (AD) of waste wafers (WF - control) and co-substrate system - waste wafers and cheese (WFC - control), combined with digested sewage sludge. The aim of the study was to evaluate the physicochemical parameters of the chitosan/perlite (Ch/P; 3:1) carrier material and to verify its effect on the directions of change of the bacterial microbiome, removal kinetics of organic matter and AD process efficiency. The experiment was conducted in a laboratory, in a periodical mode of operation of bioreactors, under mesophilic conditions. The results of analyses of morphological-dispersive, spectroscopic, adsorption, thermal and microbiological properties confirmed that the tested carrier material can be an excellent option to implement in biotechnological processes, especially in anaerobic digestion. The microstructural properties of the carrier were influenced by both components: perlite determined the development of the specific surface area, while chitosan shaped the porosity of the system. The thermal properties were determined by the less heat-resistant component, present in a threefold higher weight proportion, i.e., chitosan. The evaluation of quantitative and qualitative changes in the genetic diversity of bacterial communities, carried out using Next Generation Sequencing (NGS), showed that the material has a modifying effect on the bacterial microbiome. Amount of bacteria from phyla Actinobacteria, Bacteroidetes, Campilobacterota, Chloroflexi, Euryarchaeota, Planctomycetes, and Proteobacteria decreased while Firmicutes, Synergistetes, and Thermotogae increased during the course of the experiment. The shapes of the FT-IR spectra indicated a dependence of the degradation rate on both the presence of the carrier and the cosubstrate system. Monitoring of the course of AD was carried out by measuring key parameters for the stability of the process: pH, VFA and VFA/TA ratio (volatile fatty acids/total alkalinity). As a result, an increase in the volume of biogas/methane produced, under the influence of the carrier, was recorded for WF-control by 12.05% and for WFC-control by 19.16%. The volume of methane for the WF-control increased from 351.72 $m^3 Mg^{-1}$ VS to 411.14 $m^3 Mg^{-1}$ VS, while for the cosubstrate sample it increased from 476.84 $m^3 Mg^{-1}$ VS to 518.08 $m^3 Mg^{-1}$ VS, confirming the validity of combining the respective cosubstrate with microbial carrier in anaerobic bioreactor.

Keywords: chitosan/perlite system; physicochemical properties; impact of additives; anaerobic digestion; FTIR spectroscopy; NGS analysis

 doi:10.20944/preprints202406.0813.v1

1. Introduction

Anaerobic digestion (AD) is a complex process consisting of a number of microbial transformations, whereby organic substrates are converted into so-called biogas containing mainly methane and carbon dioxide. This anaerobic decomposition of organic matter is currently used for the treatment of wastewater, sludge in wastewater treatment plants and slurry [1]. It is also increasingly being used to generate energy from various origins of agri-food waste, which is gradually displacing plant substrates from purpose-grown crops [2,3]. The microbial community in an anaerobic reactor comprises three typical populations: fermentation bacteria, acetic bacteria and methanogenic bacteria. Of these, methanogenic bacteria are the most sensitive to changes in environmental conditions due to their slower growth compared to fermentative and acetic bacteria [4].

Due to the importance of the density and species of methanogenic bacteria in AD, special emphasis is placed on developing and maintaining a stable and active population of methanogenic bacteria [5]. To this end, microbial carriers are used in biotechnological processes, including AD. Bacteria and archaeons involved in methanogenesis potentially form biofilms by adhering or attaching to the carrier material. Properly selected biofilm carriers prevent the leaching of microorganisms from sludge [6], ensure the maintenance of a high density of methanogens and, consequently, highly efficient methane production. Thus, biofilm carriers in AD reactors have the potential to increase reactor productivity [7]. The characteristics of an ideal cell carrier are mainly: developed specific surface area, porosity, biocompatibility, stability, low density and mechanical strength [8]. In addition, the carrier should be cheap in practical applications (e.g., as a waste material) and should be non-toxic to cells for both the immobilised material and the environment.

To date, many types of biofilm carriers have been developed for the AD process, in the form of stand-alone materials and suitable systems, performing specific functions and manifesting both advantages and some disadvantages (e.g., small pore diameters, dissolution, low efficiency, high cost, low availability). Immobilisation of microorganisms on various types of zeolites has been assessed as beneficial [9]. In general, zeolites are the materials most commonly used as carriers in the AD process, due to their favourable characteristics for microorganism adhesion and their ability to remove ammonium ions [10–12]. In research work carried out with carrier materials of various origins, successful results in the form of improved process performance were most often reported. The increase in methane generation efficiency has been explained by the effective action of the aforementioned biofilm carriers in terms of, among other things: making the bacteria resistant to changes in environmental conditions, stabilising the system, reducing the release and action of inhibitors and increasing the degree of substrate biodegradation. It has been suggested that promoting surface contact and improving interspecies electron transport (when using conductive materials such as magnetite) has had a huge impact on treatment results [13,14]. Modern spectroscopy techniques and next-generation sequencing provide information on biofilm composition and structural organisation, explaining the function of the added material [15–17].

The development of technologies using microbial carriers used in anaerobic degradation is therefore needed and justified. The authors, guided by previous experience and research results, have developed another system to support the AD process, based on interesting, previously unused materials: chitosan and perlite.

Chitosan is a natural product derived from chitin, which is most commonly found in the exoskeletons of shrimps and crabs and in lobster shells. Like chitin, chitosan is a linear polysaccharide. It is a polycationic polymer, consisting of two types of units: an N-acetyl-d-glucosamine unit together with a d-glucosamine unit, with the arrangement of these units depending on the proportion of acetylated fragments. Chitosan has two hydroxyl groups and one amino group in its glycosidic residue. This compound is noted as a particularly efficient and inexpensive biosorbent (compared to activated carbon), as well as due to its high content of functional hydroxyl and amino groups [18–20]. Chitosan possesses a number of valuable physicochemical properties, such as biocompatibility, non-toxicity, ability to form polycations in acidic media, and ease of modification [21]. These features make it applicable in medicine and pharmacy, various types of

 doi:10.20944/preprints202406.0813.v1

industries, environmental protection, water purification processes, various types of separation processes, etc. It is worth mentioning that nano chitosan, compared to traditional microporous materials used in separation, is characterised by better performance, which can be attributed to its developed specific surface area and higher adsorption capacity [22,23]. According to the literature, some studies have already been carried out, demonstrating the strong biocatalytic effect of chitosan and chitosan-magnetite and chitosan-titania-magnetite systems on biogas production and methanogenic activity [24–26]. It should be noted that chitosan does not exhibit all the characteristics of a universal microbial carrier (it swells in water, is not mechanically robust), but can nevertheless effectively influence the course and efficiency of the AD process due to its morphological, microstructural and chemical properties.

Perlite, on the other hand, is an interesting mineral material — it is a magmatic rock, composed of acidic rhyolitic volcanic glaze. Chemically, perlite is a hydrated sodium-potassium aluminosilicate, containing 68—73% silica SiO_2, 10—12% alumina Al_2O_3, as well as oxides of sodium, potassium, magnesium, calcium and iron. The extracted perlite is ground and roasted at 900–1100°C. Interestingly, water droplets encapsulated in the grains produce steam at a pressure that crushes the material. In parallel, a process of sintering the volcanic glaze takes place, causing the mineral grains to expand [27,28]. Perlite is widely used in construction and horticulture. It is a base product or additive for the manufacture of insulation materials — thermal and acoustic — and construction materials. Expanded perlite particles have an irregular spherical shape with an intensely ribbed surface. The characteristic irregular, porous microstructure of perlite ensures good adhesion and has also resulted in it being studied and used as a microbial carrier in construction — in extending the service life of concrete structures [29,30]. Furthermore, perlite is chemically inert, non-toxic, mechanically stable, insoluble in water and inexpensive. Regarding the use of mineral carriers in anaerobic digesters, it should be noted that many types have been studied so far, including bentonite, sepiolite, talc, vermiculite, montmorillonite, and diatomite. Some of these carriers have been found to facilitate startup, while others contribute to COD (chemical oxygen demand) removal [31]. Perlite has so far been used rarely, nevertheless Ivankovic et al., 2022 proved through their research that it can successfully act as a microbial carrier in the AD process [32]. The researcher used this aluminosilicate material as an additional support in the decomposition of lignocellulosic waste in the form of olive cake. As a result of the increased immobilisation of cells on the carrier, increased primary substrate degradation and accelerated the augmentation process were observed. This evidence prompted the implementation of studies involving perlite.

The main objective of this work was to evaluate the effect of a previously unused microbial carrier in the form of a chitosan/perlite system (3:1) on the stability and performance of anaerobic digestion of food waste (in a batch reactor, mesophilic conditions). Changes in microbial diversity following the influence of the added carrier (in-process) were also assessed, as well as qualitative changes in the molecular structure of the decomposed materials and quantitative changes, using next-generation sequencing (NGS), FT-IR infrared spectroscopy and the classical drying and weighing method, respectively. The paper also presents the results of analyses of the most relevant physicochemical parameters of the studied carrier, including morphological and thermal properties, as well as chemical composition, porosity and specific surface area development.

2. Materials and Methods

2.1. Feedstocks and Additional Materials

In the conducted studies, selected confectionery waste in the form of pieces of filled wafer waste (WF) was used as substrates, both on their own and in combination with cheese waste, such as curd (C), as a co-substrate. Both feedstocks were supplied from production companies in the vicinity of Poznań (Wielkopolskie Voivodeship). On the other hand, digested sewage sludge, taken — similarly to other experiments performed by the author — from the municipal sewage treatment plant of the city of Poznań [33–35], was used as inoculum. The basic physicochemical parameters of these materials are presented in Table 1.

 doi:10.20944/preprints202406.0813.v1

Table 1. Physicochemical properties of feedstocks and inoculum.

Materials	pH	Cond.	TS	VS	C/N ratio	C	N	$N–NH_4^+$	P_{total}
	–	(mS cm^{-1})	(wt %)	(wt $\%_{TS}$)	–	(wt $\%_{TS}$)	(wt $\%_{TS}$)	(wt $\%_{TS}$)	(wt $\%_{TS}$)
Wafers	7.02	1.62	73.24	96.81	37.50	42.37	1.13	0.36	0.15
Cheese	4.32	72.96	34.25	92.56	3.60	45.87	12.73	0.53	1.62
Inoculum	7.93	26.50	3.47	71.43	11.21	33.06	2.95	2.48	2.57

Cond. – conductivity, TS – total solids, VS – volatile solids.

Additional materials, acting as microbial carriers in the AD process carried out, included chitosan from crab shells (highly viscous) from Sigma-Aldrich, Saint Louis, Missouri, USA, and perlite, which is an amorphous mineral consisting of fused potassium aluminium sodium silicate (Biomus sp. z o.o., Lublin, Poland). Both materials were purchased in powder form and combined in a weight ratio of 3:1 (chitosan/perlite, Ch/P). Both substances were placed in the bioreactor in the amount of 20 g per 1 L of feedstock, following the positive effects observed in previous research studies [36,37].

Figure 1. Microbial carrier in the form of a chitosan/perlite (3:1) substance system.

The physicochemical properties of the constituent materials of the carrier and the system are detailed in Results and Discussion.

2.2. Physicochemical Analysis of Substrates and Carriers

2.2.1. Analysis of Feedstocks, Inoculum and Batches

For feedstocks, inoculum and batches, pH (potentiometric analysis) and electrolytic conductivity were measured using an Elmetron CP-215 apparatus (ELMETRON, Zabrze, Poland). Their total solids (TS) were determined by drying at 105 °C (Zalmed SML dryer, Zalmed, Łomianki, Poland) and volatile solids (VS) by combustion at 550 °C (MS Spectrum PAF 110/6 furnace, MS Spectrum, Warsaw, Poland) – gravimetric analysis.

The substrates were also tested for carbon content — combustion at 900 °C followed by CO_2 determination (Infrared Spectrometry, OI Analytical Aurora 1030W TOC Analyzer, Picarro Inc, United States); nitrogen content — titration, Kjeldahl method using 0.1 n HCl, with Tashiro's indicator; ammonium nitrogen concentration — distillation and titration method, with the use of 0.1 n HCl, in the presence of Tashiro's indicator, and phosphorus content — mineralisation with nitric acid in an UltraWAVE microwave mineraliser from Milestone Inc. (Fremont, California, USA),

 doi:10.20944/preprints202406.0813.v1

followed by spectrophotometric analysis with Varian Cary 50 (Varian Inc., Palo Alto, California, USA) [38].

2.2.2. Analysis of Carrier Materials

Carrier materials, individually as well as in a chitosan/perlite (3:1) binary system, were characterised for their physicochemical and microstructural properties.

As a first step, the size of particles of the materials was analysed using a Zetasizer apparatus equipped with a 4 mW helium/neon laser (Zetasizer Nano ZS, Malvern Instruments Ltd., UK). This apparatus measures particles with sizes from 0.6 to 6000 nm (non-invasive backscattering technique — NIBS). Prior to the analysis all samples were dispersed in isopropanol using mild sonication. All the measurements were performed at 25 °C. Cumulants analysis gives a width parameter known as the polydispersity, or the polydispersity index (PdI). The cumulant analysis involves fitting a polynomial to the logarithm of the G1 correlation function:

$$ln[G1] = a + bt + ct^2 + dt^3 + et^4 + \ldots \quad (1)$$

The value of b is known as the second order cumulant, or the z-average diffusion coefficient. The coefficient of the squared term, c, when scaled as $2c/b^2$, is known as the polydispersity [39,40].

The morphology and microstructure of the PLA were examined on the basis of SEM (scanning electron microscope) images recorded from a scanning electron microscope FEI Quanta FEG 250 (FEI Company, Hillsboro, OR, USA). The microscope operates in low vacuum mode at a pressure of 70 Pa and an accelerating voltage of 10 kV. Before testing, the samples were coated with Au for 5 seconds using a Balzers PV205P coater (Balzers, Switzerland) [41]. The EDS (energy dispersive X-ray spectroscopy) analysis was carried out with the beam accelerating voltage of 10 kV, using the EDS Octane SDD (EDAX Inc., Mahwah, NJ, USA) detector. The contents of elements such as C, O, and Si were analysed.

The chemical composition of the samples was determined using an elemental analyser FLASH 2000 (Thermo Fisher Scientific, Waltham, USA), which operates based on dynamic combustion technology. Initially, samples are weighed in tin capsules (approx. 2–4 mg) and placed in the reactor with an autosampler with a specific amount of oxygen. After combustion at 900–1000 °C, the combustion gases are transported in a helium flow to the second furnace of the reactor, filled with copper and then, through a water trap, to a chromatography column, which separates the individual products. Finally, the separated gases are detected using the Thermal Conductivity Detector (TCD). The Thermo Scientic Eager Xperience data analysis software automatically generates and displays a report at the end of the measurement cycle. In contrast, the instrument performs oxygen analysis in pyrolysis mode. Samples are weighed in silver capsules and placed in the furnace with an autosampler. The reactor contained nickel-coated carbon and its temperature is maintained at 1060 °C. The oxygen in the sample combined with carbon to form carbon monoxide, which was subsequently chromatographically separated from the other products and measured by a TCD detector [40,41].

To determine the porous structure parameters, nitrogen adsorption/desorption isotherms at 77 K and parameters such as surface area (A_{BET}), total volume (V_P) and mean size (S_P) of pores were determined using an ASAP 2420 instrument (Micromeritics Instrument Co., Norcross, USA). Prior degas was performed at the temperature of 90°C under vacuum conditions. The specific surface area (SSA) was calculated on the basis of the Brunauer–Emmett–Teller (BET) model used for a linear part of the adsorption isotherm ($0.05<P0<0.25$). The BJH (Barrett–Joyner–Halenda) method was used to determine the mean pore size and volume [40,41].

In order to obtain the infrared absorption spectrum of the powders studied, Fourier Transform Infrared Spectroscopy (FT-IR) measurements were performed on a Vertex 70 spectrophotometer (Bruker, Bremen, Germany) at room temperature. The sample was analysed, in the form of tablets, made by pressing a mixture of anhydrous KBr (ca. 0.25 g) and 1 mg of the tested substance in a special steel ring under a pressure of approximately 10 MPa. FT-IR spectra were obtained in the transmission mode between 4000 and 400 cm^{-1}. The analysis was performed at a resolution of 0.5 cm^{-1} [37,41].

 doi:10.20944/preprints202406.0813.v1

Thermal changes in the test materials occurring with controlled temperature rise and fall were observed by performing differential scanning calorimetry (DSC) measurements, using the Netzsch DSC 204 F1 Phoenix (Selb, Germany) calorimeter. The actual measurement consisted of two steps: in the first step, the samples (each ca. 5 mg) were heated up from 25 °C up to 500 °C at a rate of 10 °C /min under a nitrogen atmosphere and maintained at this temperature for 5 minutes. In the second step, the samples were cooled from 500 °C to 20 °C, also in a nitrogen flow (10 mL/min) [41].

2.3. Biogas Production Set-Up

2.3.1. Batch Preparation

Control samples — prepared with the use of waste wafers (WF) alone and a system of co-substrates of wafers and waste cheese (WFC) — were tested: WF – control, WFC – control and for samples with the addition of Ch/P carrier: WF + DEP and WFC + DEP. The composition of the batches was determined based on the German standard VDI 4630 [42], according to which the dry matter content of the mixtures did not exceed 10% [33,34]. The composition of the batches along with the most relevant physicochemical parameters for the process is presented in Table 2.

Table 2. Composition and selected parameters of the substrate/inoculum samples.

Samples	**WF** (g)	**CE** (g)	**Ch/P** (g)	**Inoc.** (g)	**pH**	**Cond.** (mS cm^{-1})	**TS** (%)	**VS** (%)
WF – control	9.5	–	–	835.5	7.16	62.95	4.08	73.46
WF – Ch/P	9.5	–	20.0	835.5	7.03	69.25	3.97	72.62
WFC – control	6.5	3.0	–	833.0	6.91	77.54	4.15	69.38
WFC – Ch/P	6.5	3.0	20.0	833.0	6.83	78.86	4.23	68.55

WF – wafers, CE – cheese, Ch/P – chitosan/perlite, cond. – conductivity, TS – total solids, VS – volatile solids.

2.3.2. Anaerobic Digestion

Anaerobic digestion was carried out in a multi-chamber bioreactor, shown in Figure 2. The total number of digesters in this experiment was 12. Each of the 4 samples was tested three times.

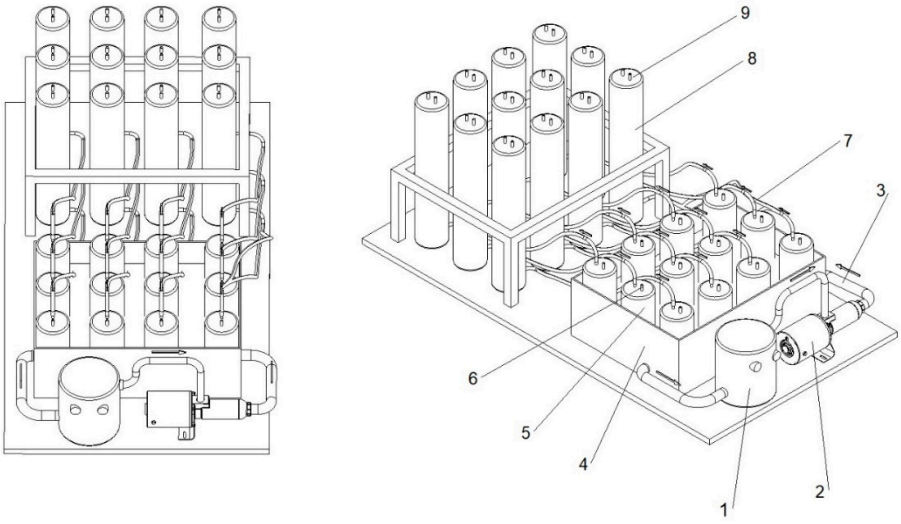

 doi:10.20944/preprints202406.0813.v1

Figure 2. The anaerobic bioreactor (12-chamber section) used in biogas production experiment: 1 – water heater; 2 – water pump; 3 – insulated tubes for heating; 4 – water jacket (39 °C); 5 – bioreactor (1.4 L); 6 – slurry sampling valve; 7 – tube for biogas transport; 8 – graduated tank for biogas; 9 – gas sampling valve [36].

The 1.0 L bioreactors (5) were filled in with a substance that was stirred once a day. The bioreactors were placed in a container with water (4), connected to a heater (1), which allowed to perform the process at a set range of temperatures (mesophilic conditions). The produced biogas was directed (7) into tanks (8) (with a scale) where it was stored [36].

The hydraulic retention time (HRT) was 20 days. As per the German standard DIN Guideline 38 414-S8 (DIN, Deutsches Institut für Normung) [43], the experiment was carried out until the daily biogas production fell below 1% of the total biogas produced, in all bioreactors. The volume of biogas produced was measured every 24 h. The concentration of methane, carbon dioxide, hydrogen sulphide, ammonia and oxygen in the biogas was measured using a Geotech GA5000 gas analyser (Geotech, Coventry, UK). The gas concentration was measured with Mg–72 and Mg–73 measuring instruments by Alter inc., Tarnowo Podgórne, Poland. The gas analyser measures gas concentrations within the following ranges: 0–100% CH_4, 0–100% CO_2, 0–25% O_2, 0-2,000 ppm H_2S, and 0–1,000 ppm NH_3. Assessment of biogas yield (in m^3 Mg^{-1}), in terms of total solids and volatile solids, was performed based on experimental data. In the case of bioreactors with batch control and with batch along with a carrier, the total amount of biogas was calculated based with the use of formulas that had been described in the previous works of the authors [33,34,38,40].

2.3.3. Physicochemical Analysis of Samples Collected

In addition to measuring the pH of the fermenting suspension samples collected during the process (methodology as in subchapter 2.2.), the concentration of VFA (volatile fatty acids), TA (total alkalinity) and then the VFA/TA ratio (volatile fatty acids-to-total alkalinity ratio) were determined for the same samples. For this purpose, 5 mL of a given sample was collected, titrated by 0.1 N of sulfuric acid solution (H_2SO_4) up to pH 5.0 to calculate the TA value. The VFA value was obtained after a second titration between pH 5.0 and pH 4.4 [38].

The collected samples were additionally subjected to FT–IR analysis in order to visualise changes in the chemical structure of the samples and to obtain information on the dynamics of organic matter decomposition during the AD process (methodology as in subchapter 2.2.2). The collected samples were continuously prepared for analysis by undergoing a drying process in a stationary laboratory dryer, SLN 75 (POL–EKO sp.k.). Wodzisław Śląski, Poland), at a temperature of 105°C for 48 hours, until a powdered form was obtained. After weight analyses and FT-IR analyses, the samples were calcined in NT 1313 laboratory furnace (Neoterm, Wrocław, Poland) at 550 °C for 2 hours to determine the mass of organic matter.

2.3.4. Microbiological Analysis of Samples Collected

In order to investigate and compare qualitative and quantitative changes occurring during the in anaerobic bioreactor process, control and Ch/P carrier samples were analysed using Next-Generation Sequencing (NGS) analysis, as in previous research work [17,44]. The material collected from the bioreactors during the first and last phases of the process was designated as follows: WF–Control 1, WF–Control 2, WF–Ch/P 1, WF–Ch/P 2, WFC–Control 1, WFC–Control, WFC–Ch/P 1 and WFC–Ch/P 2.

DNA Extraction and Next-Generation Sequencing (NGS) Total DNA was extracted from 500 mg of each sample using Genomic Mini AX Soil kit (A&A Biotechnology, Gdynia, Poland) according to the manufacturer's instruction. The extracted DNA was quantified using the Quant-iT HS ds.-DNA assay kit (Invitrogen, Carlsbad, CA, USA) on a Qubit2 fluorometer (Invitrogen); 2 µL of extracts were analysed using a 0.8% agarose gel. The metagenomic analysis was based on the V3-V4 hypervariable region of the 16S rRNA gene. Specific primers 341F and 785R were used for amplification of this region and library preparation. The polymerase chain reaction (PCR) was performed using the Q5

 doi:10.20944/preprints202406.0813.v1

Hot Start High-Fidelity DNA Polymerase Kit (NEB Inc., Ipswich, MA, USA) under reaction conditions according to the manufacturer's specifications. The sequencing was performed by means of a MiSeq sequencer in 2 × 250 bp paired-end (PE) technology, 14, 4429 7 of 23 using Illumina v2 chemistry kit [17]. The reactions were performed according to the Illumina V3-V4 16S RNA amplification protocol (Illumina, Inc., San Diego, CA, USA), while sequencing was carried out according to Illumina MiSeq PE300 software (Genomed S.A., Warsaw, Poland). The automated data analysis was performed on MiSeq and in Illumina's Cloud BaseSpace environment, using the 16S Metagenomics protocol (ver. 1.0.1). The libraries were prepared similarly according to the attached Illumina protocol.

All bioinformatics analyses were performed using R software (version 3.6.0) [45] with the DADA2 package (version 1.14) [46]. The learnErrors function was used for error rate estimation, dada for identifying exact sequence variants, and removeBimeraDenovo for removing chimeric sequences. Based on the quality graphs, the last 20 forward and 20 or 80 reverse bases were truncated. The RDP (Ribosomal Database Project) v18 [47] was used for taxonomy assignment using IDTAXA [48]. The results were implemented into the phyloseq (1.22.3) package [49].

3. Results

3.1. Physicochemical Properties of Carrier Materials

3.1.1. Morphological and Microstructural Characteristics

SEM microscopic images taken at various magnifications (see Figure 2a–i) demonstrate the morphological and microstructural characteristics of chitosan (Figure 2a,b,c), perlite (Figure 2d,e,f), as components of the carrier material shown in the images of Figure 2g,h,i. Images of pure chitosan showed a heterogeneous surface with numerous grooves and indentations (Figure 2b,c), characteristic of crustacean carapaces [50]. Microscopic images of perlite show a porous, spongy (Figure 2e) microstructure, formed by the passage of this material from liquid magma (during volcanic eruptions) into seawater [51]. In water, the perlite solidifies instantly, which causes the vapour bubbles within it to close, hence the holes and cracks seen in the images (Figure 2f).

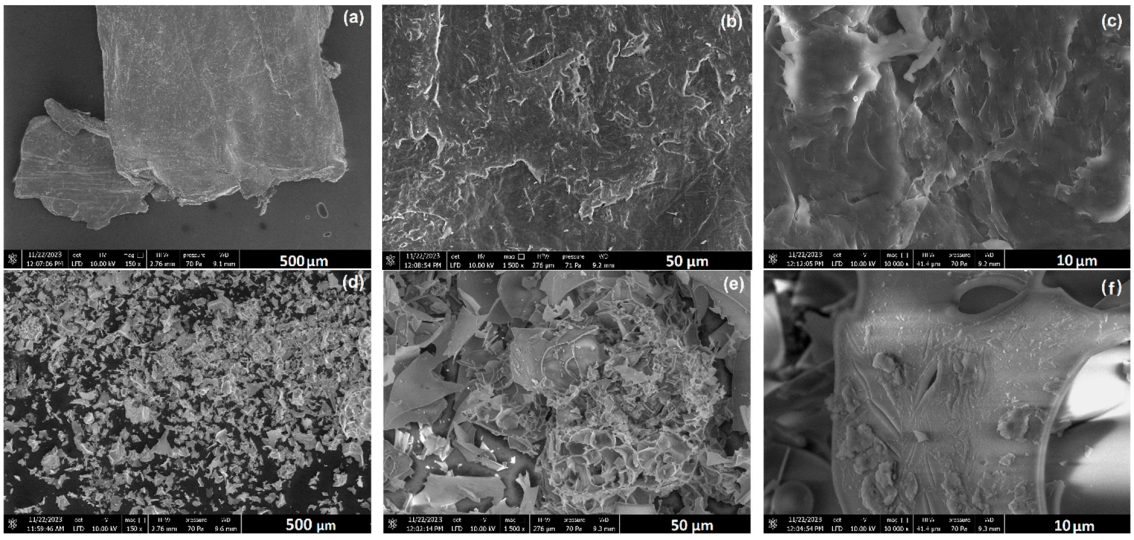

 doi:10.20944/preprints202406.0813.v1

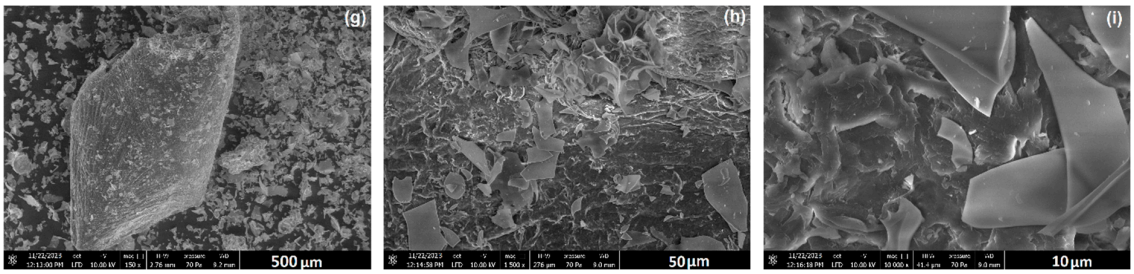

Figure 2. SEM images of chitosan (a), (b), (c), perlite (d), (e), (f), and chitosan/perlite system (g), (h), (i) at various magnifications.

The result of combining the two materials in a 3:1 ratio (with a predominance of chitosan) was a highly heterogeneous, in places rough microstructure with discernible aggregates and agglomerates of particles [52]. The formed niches provide an ideal point for cell immobilisation. This characteristic and functional microstructure of the chitosan/perlite system has been used previously (chitosan-coated perlite) as a biosorbent in the removal of impurities [53,54]. The formation of cross-linked chitosan/perlite composites increased the sorption capacity of chitosan [55].

Average diameters, measured by Zetasizer, of chitosan particles and were 2605 nm, where 48.1% were 957.1 nm particles. The high PdI index value of 0.892 indicates the presence of significant particle agglomerates in the sample. These results confirm a highly heterogeneous powder microstructure with micrometre-sized particles. The results are similar for perlite, for which the Z-Average reading is 1242 nm (particles with diameters of 508.7 nm cover 56.3% of the sample) and PdI=0.655. The sample of the chitosan/perlite system maintains the tendency to form particles with significant size (Z-Average 1785 nm) and high PdI value (0.855). The results obtained are in agreement with literature data, where micrometer-sized powders were used in the study [51,56]. Nguyen et al., 2017 observed in their study the dependence of chitosan particle size and size distribution on the zeta potential value. They found that larger particle diameters could result in a decrease in the zeta potential value, implying lower dispersion stability [57].

3.1.2. BET Surface Area and Pore Structure

The microstructural structure of materials has a direct impact on the development of the specific surface area, which is a key parameter of cell carriers. Figure 3a,b shows the nitrogen adsorption/desorption isotherms for three samples: chitosan, perlite and the chitosan/perlite system. The nature of the isotherms indicates their mesoporous structure. The amount of nitrogen adsorbed by the samples up to a relative pressure p/p_0 of 0.8 increased slightly. Above this value, as indicated by the shape of the isotherms, the amount of nitrogen adsorbed by the materials increased rapidly, reaching the highest value for perlite, followed by the chitosan/perlite carrier, and the lowest for chitosan. The results were hereby favoured by the spongy and porous structure of perlite (see Figure 3b), which, together with the smaller particle size (compared to chitosan), favourably influenced the development of the specific surface area. Smaller particle diameters in the materials develop the specific surface area (especially the nanoparticles) to a large extent and shape their specific and unique properties [39]. As the results in Table 3 show, it is perlite that has the highest BET surface area value (1.3730 m^2/g) and pore volume (0.002678 cm^3/g).

 doi:10.20944/preprints202406.0813.v1

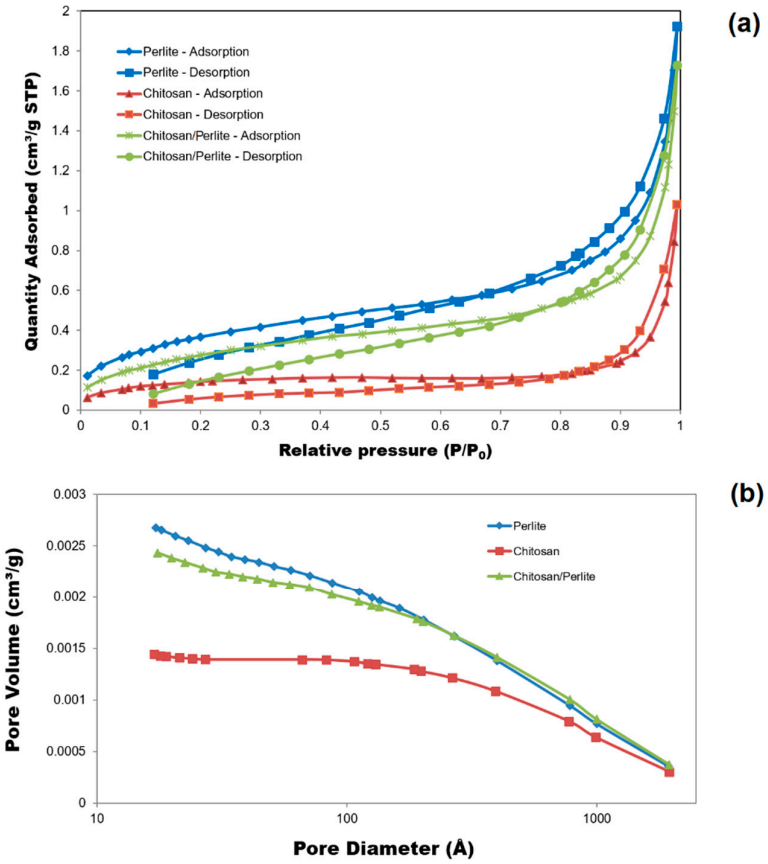

Figure 3. N_2 adsorption/desorption isotherms (a) and pore size distribution (b) of the chitosan, perlite, chitosan/perlite samples.

Given that the BET surface area of the chitosan sample was found to be the smallest (0.5061 m^2/g), it can be deduced that perlite was the decisive component for the favourable development of the microstructural properties of the carrier, in particular its specific surface area, (despite the threefold lower proportion of this component in the sample). However, the significant pore diameters of chitosan, amounting to as much as 27,366 nm, are not insignificant for the immobilisation of microorganisms. The use of a combination of both materials in numerous 'green' applications, including as a biosorbent, is therefore justified.

Table 3. Porous structure properties.

Materials	A_{BET} (m^2/g)	V_P (cm^3/g)	S_P (nm)
Chitosan	0.5061	0.001441	27.366
Perlite	1.3730	0.002678	11.842
Chitosan/Perlite	1.0746	0.002432	13.714

A_{BET} – BET surface area ; V_P – pore volume; S_P - pore diameter.

3.1.3. Elemental Analysis and FT–IR Spectra

Chitosan is chemically defined as a copolymer of 2-acetamido-2-deoxy-n -β-D-glucopyranose and 2-amino-2-deoxy-β-glucopyranose (see Figure 4a). The sorption properties of this material, towards metal ions, cholesterol and proteins, are due to the presence of reactive amine and hydroxyl

 doi:10.20944/preprints202406.0813.v1

groups in its macromolecule. Perlite, on the other hand, is a rock of volcanic origin, containing about a few percent water. Its chemical composition is shaped by the proportion of numerous oxides, where the predominant share goes to silica SiO_2 (72%) and Al_2O_3 (14%), and the remainder is made up of metal oxides, including: K_2O (4%), Na_2O (3%), Fe_2O_3 (1%), CaO (1%), MgO (0.5%), as shown by the structural formula of perlite presented in Figure 4b [21,28].

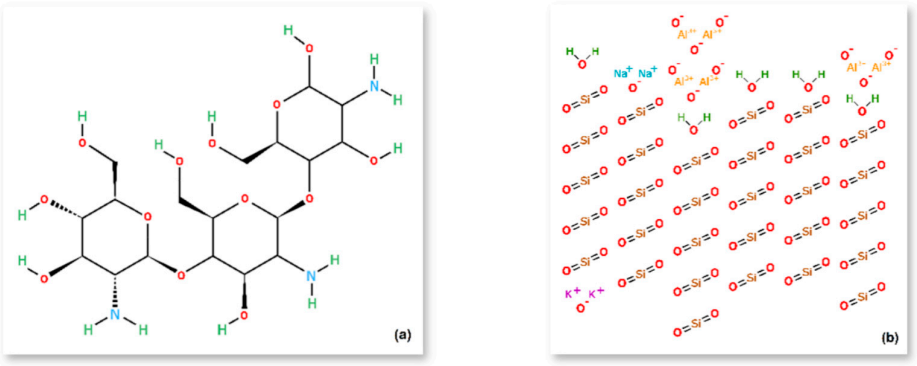

Figure 4. Structural formula of chitosan (a) and perlite (b).

The chemical composition of the components of the chitosan/perlite system and the carrier is shown in Table 4. The results of the elemental analysis confirm the contribution of four elements in chitosan, with nitrogen and aluminium present in addition to the dominant carbon and oxygen. In the case of perlite, and consequently the system of the two analysed types of material, the chemical composition is enriched with a range of other elements, both non-metals and metals (see Table 4).

Table 4. Chemical composition of the chitosan, perlite and chitosan/perlite samples.

	Elemental content, weight (%)										
Material	C K	N K	O K	Na K	Al K	Si K	S K	Cl K	K K	Ca K	Fe K
Chitosan	41.10	5.22	53.55	–	0.13	–	–	–	–	–	–
Perlite	2.14	–	48.09	2.00	7.38	34.42	0.13	0.06	4.64	0.64	0.49
Chitosan/Perlite	24.43	3.56	60.66	0.79	2.27	7.20	–	0.05	0.72	0.20	0.13

Figure 4 shows the chemical distributions of elements in the individual material samples, where, for the areas selected for analysis, a clear similarity in element distribution occurred for the perlite and chitosan/perlite system. This allows to conclude that, despite the threefold higher proportion of chitosan in the sample, it is perlite that largely shapes the microstructural properties of the carrier. This was previously observed by analysing the BET surface area (see Figure 3 and Table 3).

 doi:10.20944/preprints202406.0813.v1

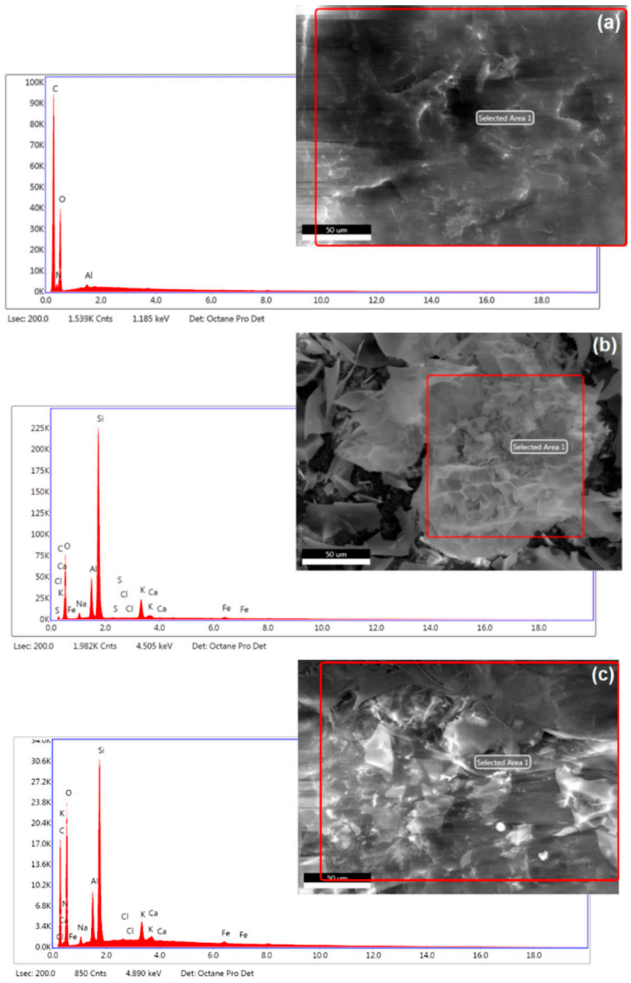

Figure 5. Chemical distributions of elements SEM-EDS of chitosan (a), perlite (b), and chitosan/perlite (c) samples.

The FT-IR spectrum of chitosan (red line) shows a broad band at 3508 cm^{-1}, corresponding to –OH stretching vibrations associated with extramolecular hydrogen bonds (see Figure 6). The stretching N–H peaks from the primary amine and the II-type amide also overlap in the same region (3500–3300 cm^{-1}). Another band absorption characteristic of chitosan appears at 1650 cm^{-1} (amide I), 1598 cm^{-1} (-NH_2 bending) and 1423 cm^{-1} (amide III). The peak for asymmetric stretch of C–O–C was identified at 1154 cm^{-1}.

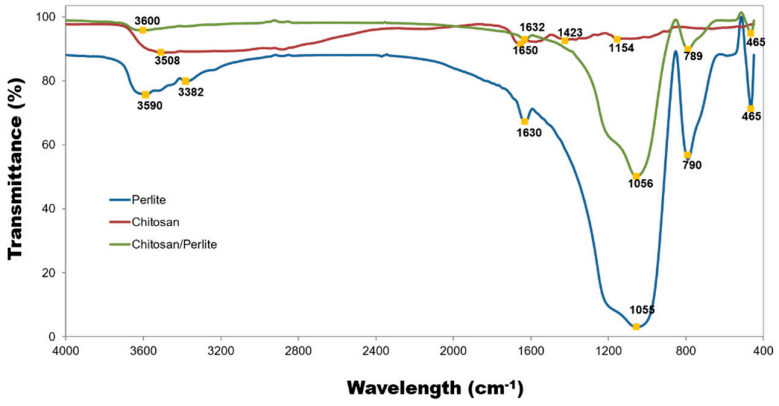

 doi:10.20944/preprints202406.0813.v1

Figure 6. FT–IR spectra of the chitosan, perlite and chitosan/perlite samples.

In the case of perlite, the peaks observed at 465 cm^{-1} and 790 cm^{-1} are due to stretching vibrations of the Si–O groups. The absorption band at about 1055 cm^{-1} is due to stretching vibrations in the Si–O–M (M: Al or Si) groups. The peak at 1630 cm^{-1} was attributed to bending vibrations of the O–H groups of the water molecules. Bands originating from water are also visible at 3382 cm^{-1} and 3590 cm^{-1}. The characterised spectrum of the perlite shows considerable similarity to that of the chitosan/perlite carrier. The results of the FT-IR analysis are largely consistent with studies performed by other researchers [28,58,59].

3.1.4. DSC analysis

DSC (Differential Scanning Calorimetry) is a technique for measuring thermal power, or more precisely, the change in the difference in heat flux arising between the test and reference samples during thermal transformation. This analysis was used to determine the thermal stability of the test microbial carrier and its components (see Figure 7a,b,c).

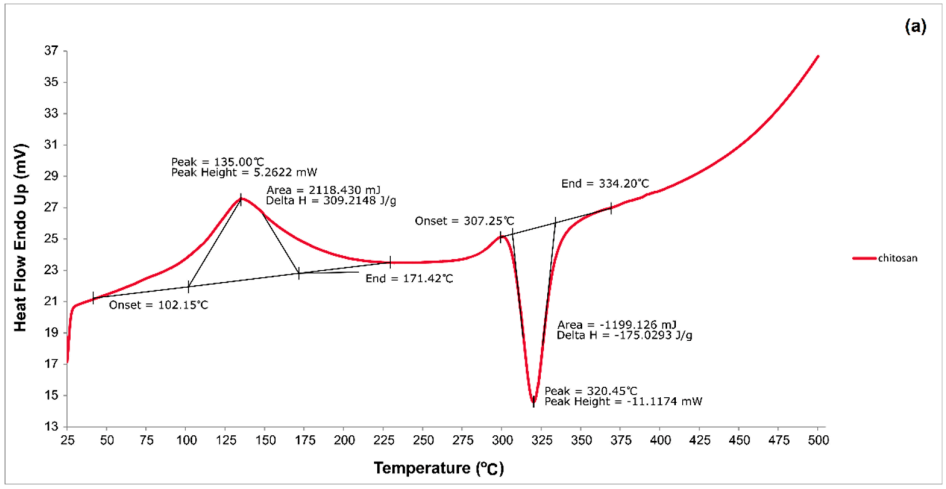

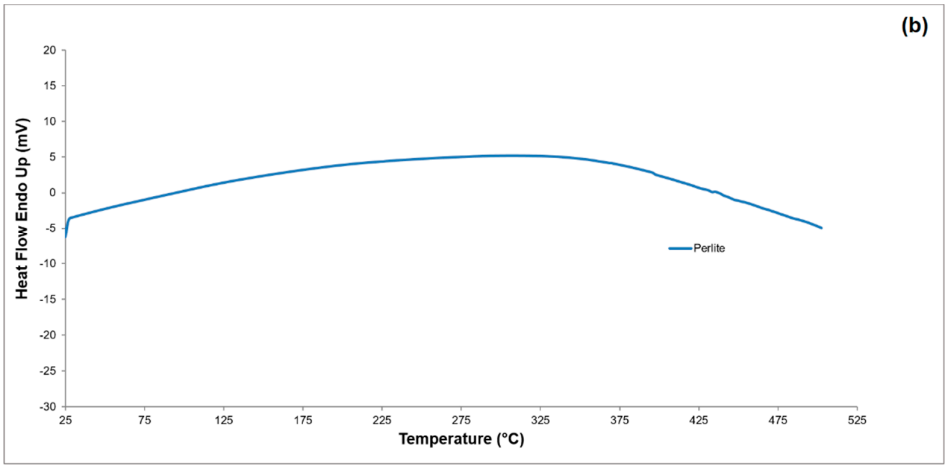

Preprints.org (www.preprints.org) | NOT PEER-REVIEWED | Posted: 12 June 2024 doi:10.20944/preprints202406.0813.v1

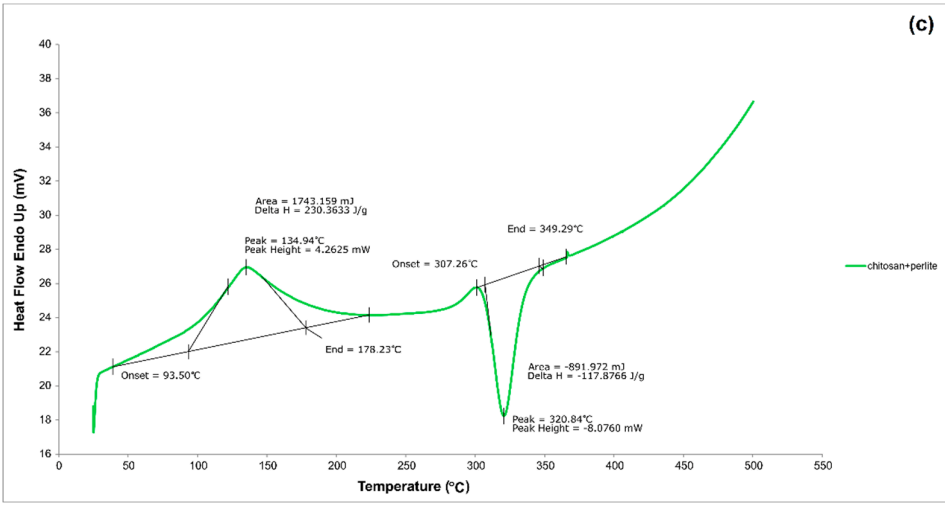

Figure 7. DSC thermograms of chitosan (a), perlite (b) and chitosan/perlite (c) samples.

Figure 7a shows a thermogram of a chitosan sample. It first shows a broad endothermic peak at 135 °C (also called dehydration temperature, TD), the presence of which is due to the evaporation of residual water bound to the hydrophilic groups of chitosan or solvent. The beginning of this peak is at about 102.15 °C and the end at about 171.42 °C. It is worth adding that, in the solid state, chitosan has a strong affinity for water and, as a result, can also undergo hydration. The presence of an endothermic peak may suggest that the bound water may not have been completely removed during drying.

A stable heat flow was observed in the chitosan sample, allowing the observation of another thermal effect (see Figure 7a) — an exothermic peak at 320.45 °C attributed to thermal degradation of chitosan (depolymerisation, saccharide ring dehydration, decomposition of deacetylated and acetylated chitosan units). The results presented are consistent with those performed by other researchers [60,61].

The DSC curve corresponding to the perlite sample clearly confirms the high thermal resistance of this material (see Figure 7b), which confirms the results of thermal analyses, including TG/DTA (Thermogravimetric Differential Thermal Analysis), carried out by other researchers [62]. No peaks indicating the degradation of perlite were observed on the thermogram throughout the entire temperature range used in the analysis. In contrast, the DSC thermogram of the chitosan/perlite system, shown in Figure 7c, is very similar to the thermogram of pure chitosan. The endothermic and exothermic peaks appear at similar temperature ranges and correspond typically to thermal transformations occurring in chitosan. Therefore, the thermal properties of the tested carrier are determined by the material that is less resistant to elevated temperatures, which has a threefold greater weight proportion. The presence of perlite apparently has no effect and generally does not change the thermal parameters, most likely due to its too low proportion.

The results obtained from the thermal analysis of the chitosan/perlite carrier proved its thermal stability over a wide temperature range, including at thermophilic and mesophilic anaerobic digestion temperatures.

3.2. Bacterial Community Abundance and Composition

The analysis of the bacterial sequencing data revealed the presence of 240 amplicon sequence variants (ASVs) of which 157 were identified at the genus level, belonging to 84 identified family taxa, 45 identified order taxa, 24 identified class taxa and 11 phylum taxa. *Clostridiaceae* and *Methanotrichaceae* were the most abundant for family taxa. Firmicutes were the most abundant phyla,

 doi:10.20944/preprints202406.0813.v1

followed by Proteobacteria and Actinobacteria (see Figure 8). The comparative analysis of the samples made it possible to examine the content of individual taxa over the course of the experiment. Similar results were obtained in studies using the diatomaceous earth/peat (DEP) cell carrier [17]. Members of Proteobacteria, Chloroflexi and Bacteroidetes are known to have traits related to wastewater treatment [63]. In addition, Firmicutes are capable to degrade a large range of substrates present in municipal sewage sludge [14,17,37].

Before the WF experiment (WF – control 1), the most abundant were Firmicutes (15.59%) and Proteobacteria (11.32%). The addition of the carrier (WF – Ch/P 1) resulted in an increase in the bacteria from the first group to 74.13% and a decrease in Proteobacteria to 2.08%. After the experiment, the control sample (WF – control 2) remained the richest in Firmicutes (62.57%) and Proteobacteria (6.33%). The amount of bacteria from the phyla Actinobacteria, Bacteroidetes, Campylobacterota, Chloroflexi, Euryarchaeota, Planctomycetes, and Proteobacteria decreased. However, Firmicutes, Synergistetes, and Thermotogae increased during the course of the experiment. The addition of the carrier (WF – Ch/P 2) resulted in increased number of bacteria from taxa Actinobacteria, Bacteroidetes, Chloroflexi, Euryarchaeota, Planctomycetes, and Spirochaetes, when compared to control sample at the same stage of the experiment (WF – control 2). During the course of the experiment, the sample with the carrier (WF – Ch/P 2) consistently maintained the highest amount of Firmicutes bacteria; however, its content decreased to 51.12% compared to the start of the experiment (WF – Ch/P 1). There was, however, an increase in the amount of bacteria of the phylum Euryarchaeota (2.72-fold increase) and Proteobacteria (2.26-fold increase). The correlations described above are similar to the results obtained in studies with both DEP and PLA (polylactide) [17,44].

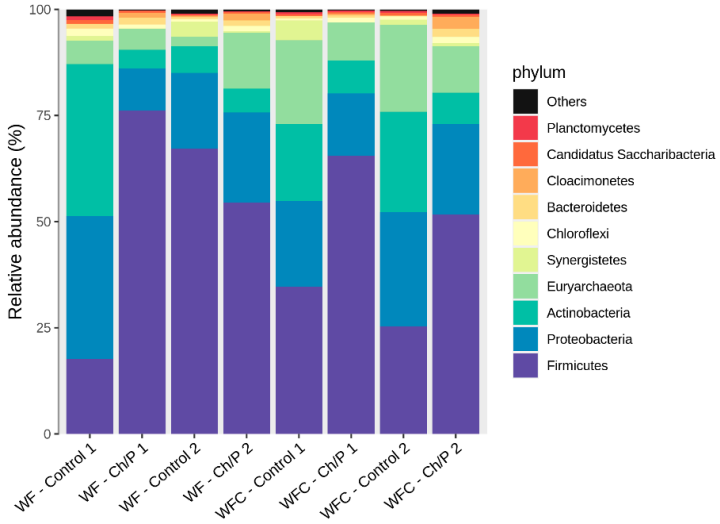

Figure 8. Composition of *phylum* taxa based on the metataxonomic analysis of the 16S rRNA gene.

Clostridium was the most abundant genus identified (present in all samples), followed by *Methanothrix* (Figure 5). In each of the experimental layouts, *Clostridium* content increased when comparing the sample with the carrier against the control. The same was observed for *Mycobacterium*, *Paraclostridium*, *Pelolinea*, and *Pseudoxanthomonas*. The increase in amount of 51 classified genera was observed in WF – ChP 1 sample, 42 in WF – ChP 2 sample, 42 in WFC – ChP 1 sample, and 38 in WFC – ChP 2 sample, in comparison to its control samples. During the course of the experiment, the amount of 43 bacterial genera increased in the WF layout, and 49 in the WFC layout. It is worth mentioning that many sequences unclassified at the genus level were also observed in our research. The highest amount of such ASVs was present in WF – ChP 2 (45.83%) and WF – Control 2 sample (45.05%). In almost all samples, most of unclassified bacteria belonged to Proteobacteria.

Preprints.org (www.preprints.org) | NOT PEER-REVIEWED | Posted: 12 June 2024 doi:10.20944/preprints202406.0813.v1

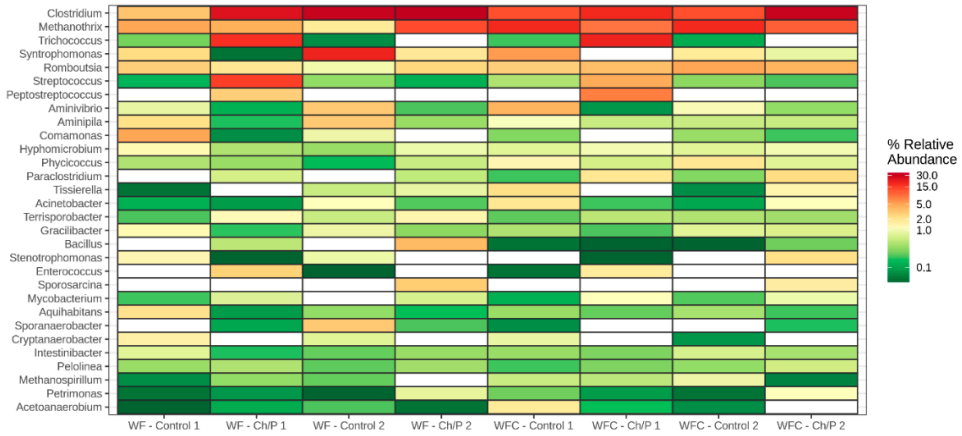

Figure 9. Composition of *genus* taxa based on the metataxonomic analysis of the 16S rRNA gene.

The MetaStat analysis indicated statistically significant differences between the control samples and samples with the addition of the carrier. Figures 10–15 show the differences in genus composition between all the analysed samples. For each chart, the number of taxa shown was limited to 30.

A comparative analysis between samples WF – Control 1 and WF – Ch/P 1 showed differences in abundance of 119 taxa (higher content of 47 bacteria in the sample with carrier) (Figure 10). A lower number of statistically significant differences (81) was found in comparison of WF – Control 2 and WF – Ch/P 2 (Figure 11).

In WFC - Ch/P 1 sample, a higher amount of 37 bacteria genus was observed, compared to WFC – Control 1 sample. The highest differences were observed for *Trichococcus*, *Macellibacteroides*, *Lacticaseibacillus*, *Longilinea*, *Limosilactobacillus*, *Falcatimonas*, *Pseudobutyrivibrio*, *Gemmobacter*, *Brevilactibacter*, *Uruburuella*, *Eubacterium*, *Erysipelatoclostridium*, *Veillonella*, *Enterococcus*, *Peptostreptococcus*, *Mycobacterium*, *Clostridium*, *Anaeroarcus*, *Desulfobulbus*, *Paraclostridium*, *Ligilactobacillus*, and *Streptococcus* (Figure 12).

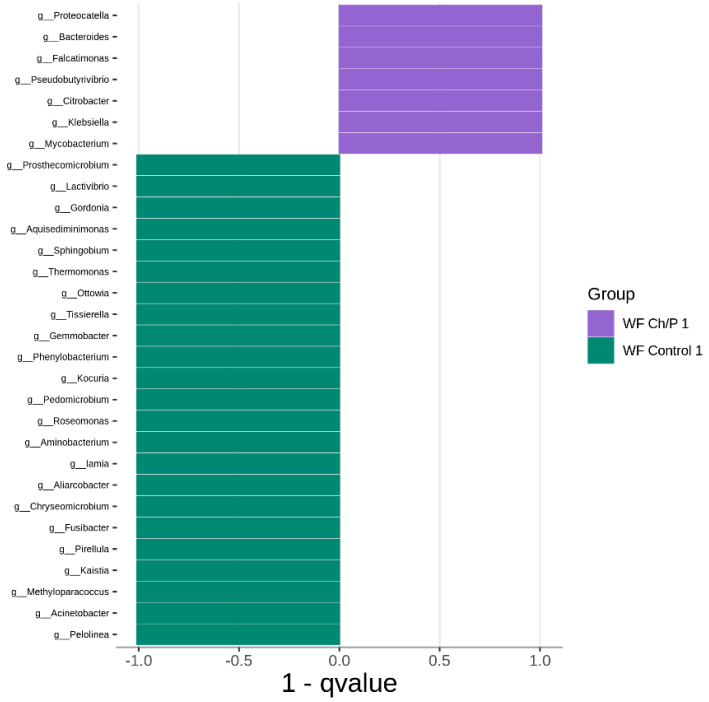

 doi:10.20944/preprints202406.0813.v1

Figure 10. Comparison (MetaStat analysis) of bacterial genus composition between WF – Control 1 and WF – Ch/P 1.

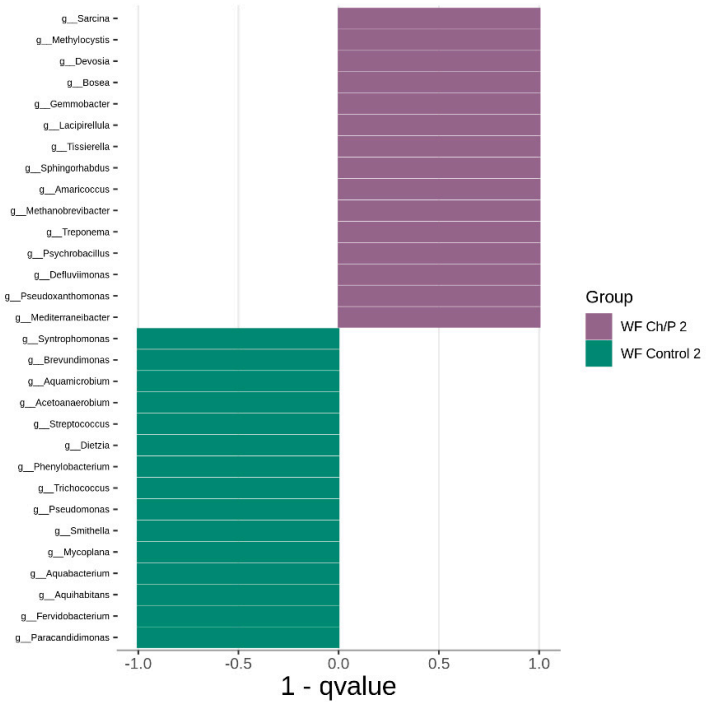

Figure 11. Comparison (MataStat analysis) of bacterial genus composition between WF – Control 2 and WF – Ch/P 2.

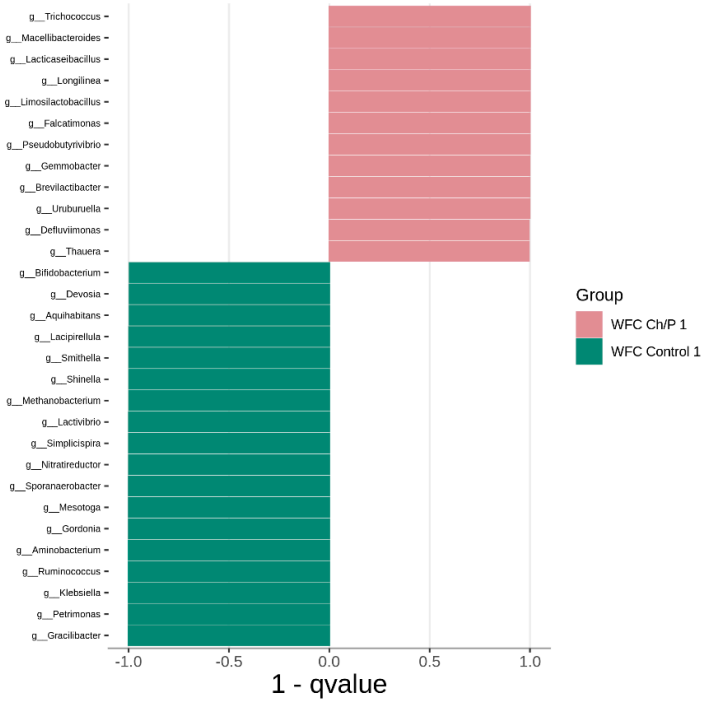

 doi:10.20944/preprints202406.0813.v1

Figure 12. Comparison (MetaStat analysis) of bacterial genus composition between WFC – Control 1 and WFC – Ch/P 1.

Among the 30 bacteria with a higher content in the sample with the addition of the carrier (WFC – Ch/P 2) compared to control sample (WFC – Control 2), the highest significance was found for the following genera: *Dietzia*, *Gemmobacter*, *Propionicimonas*, *Aminobacterium*, *Bacillus*, *Alcaligenes*, *Clostridium*, *Mycobacterium*, *Paraclostridium*, *Acinetobacter*, *Paenalcaligenes*, *Stenotrophomonas*, *Thermomonas*, *Tissierella*, *Sporosarcina*, *Fermentimonas*, *Massilibacterium*, *Pseudomonas*, *Petrimonas*, and *Sporanaerobacter* (Figure 13).

Over the course of the experiment, changes occurred that led to the appearance of differences in the content of 72 taxa in the WF samples. More taxa (39), whose abundance was statistically significantly higher, were observed in the sample taken near the final stage of the experiment (WF – Ch/P 2) (Figure 14). Almost the same observations were made for the WFC experiment (Figure 15).

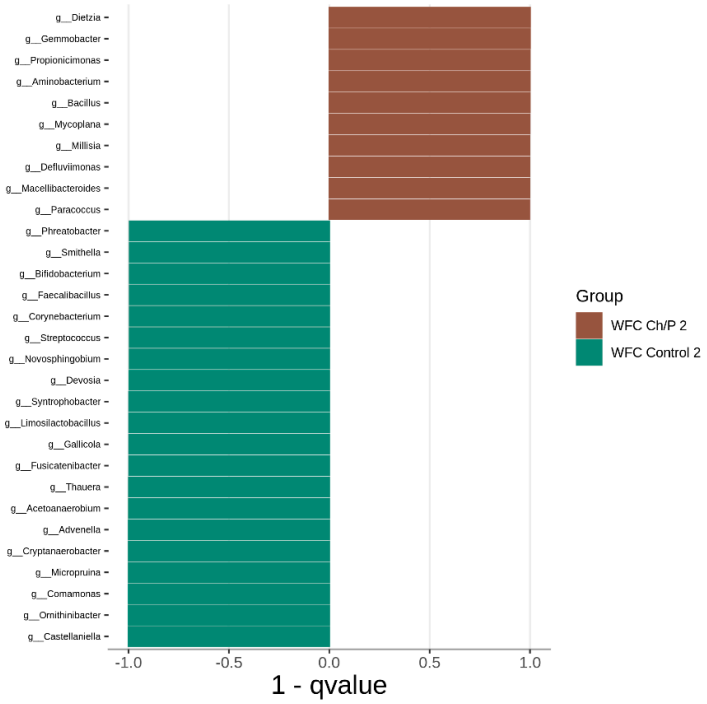

Figure 13. Comparison (MetaStat analysis) of bacterial genus composition between WFC – Control 2 and WFC – Ch/P 2.

 doi:10.20944/preprints202406.0813.v1

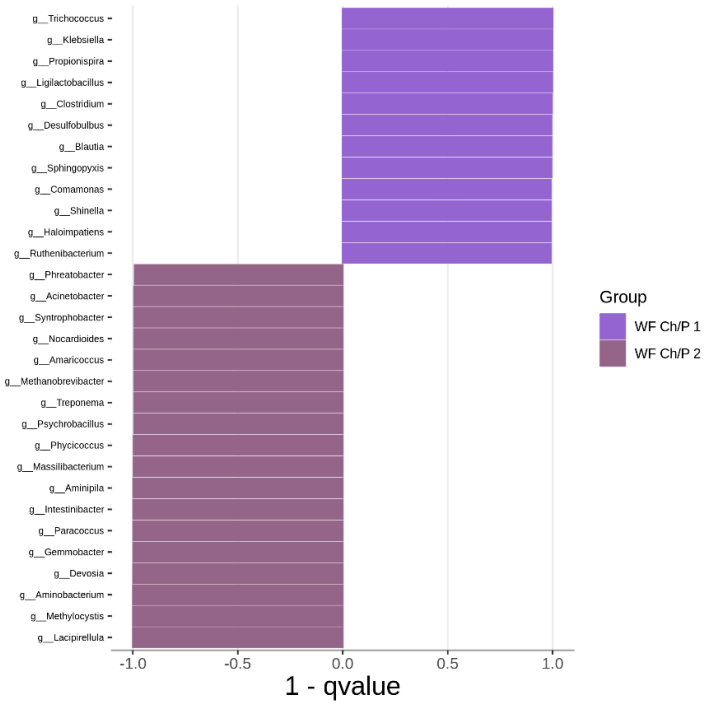

Figure 14. Comparison (MetaStat analysis) of bacterial genus composition between WF – Ch/P 1 and WF – Ch/P 2.

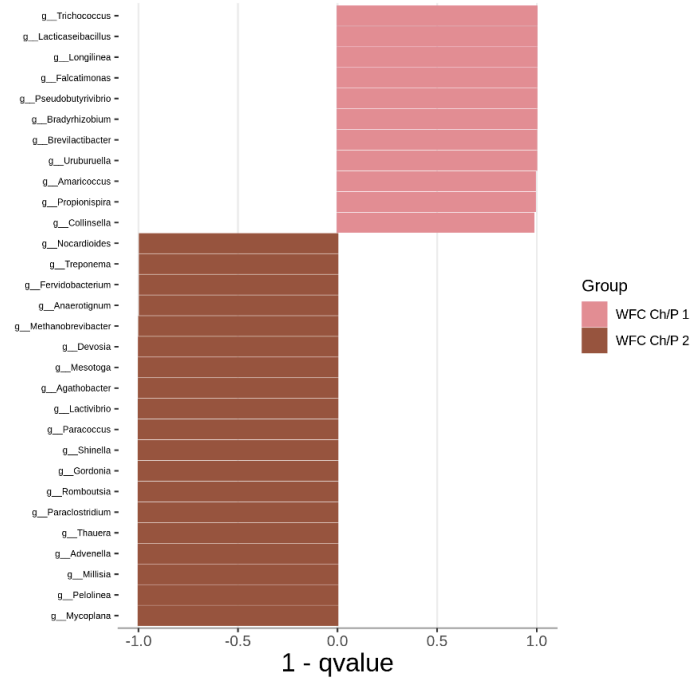

Figure 15. Comparison (MetaStat analysis) of bacterial genus composition between WFC – Ch/P 1 and WFC – Ch/P 2.

The alpha and beta diversity indices calculated from 16S rRNA sequencing data are presented in Table 5 and Table 6.

Table 5. Alpha diversity indices calculated from 16S rRNA sequencing data.

 doi:10.20944/preprints202406.0813.v1

	Chao1	Shannon	Simpson
WF – Control 1	140	3.773	0.956
WF – Ch/P 1	117	2.994	0.88
WF – Control 2	111	2.923	0.855
WF – Ch/P 2	96	2.932	0.849
WFC – Control 1	120	3.407	0.929
WFC – Ch/P 1	111	3.154	0.903
WFC – Control 2	124	3.36	0.926
WFC – Ch/P 2	105	3.24	0.882

Table 6. Beta diversity index (Bray-Curtis analysis) calculated from 16S rRNA sequencing data.

	Bray-Curtis index
WF – Control 1 vs WF – Ch/P 1	0.749
WF – Control 2 vs WF – Ch/P 2	0.466
WFC – Control 1 vs WFC – Ch/P 1	0.532
WFC – Control 2 vs WFC – Ch/P 2	0.468
WF – Ch/P 1 vs WFC – Ch/P 1	0.264
WF – Ch/P 2 vs WFC – Ch/P 2	0.228
WF – Ch/P 1 vs WF – Ch/P 2	0.509
WFC – Ch/P 1 vs WFC – Ch/P 2	0.451

The analysis revealed an abundance of 342 unique bacterial ASVs (Amplicon Sequencing Variants), most of which were present in control samples, and the core microbiome was represented by 291 ASVs (Figure 15a-f). There were 47 unique ASVs in WF Ch/P 1 sample (Figure 9a), 32 in WF Ch/P 2 sample (Figure 9b), 33 in WFC Ch/P 1 sample (Figure 9c), and 26 in WFC Ch/P 2 sample (Figure 9d), compared to the control samples. The addition of different carriers resulted in 90 ASVs in the core microbiome at the start of the experiment (Figure 9e), and 82 ASVs at the end of it (Figure 9f).

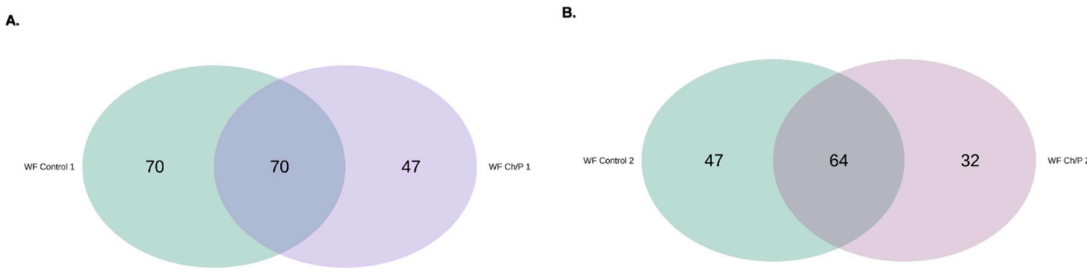

 doi:10.20944/preprints202406.0813.v1

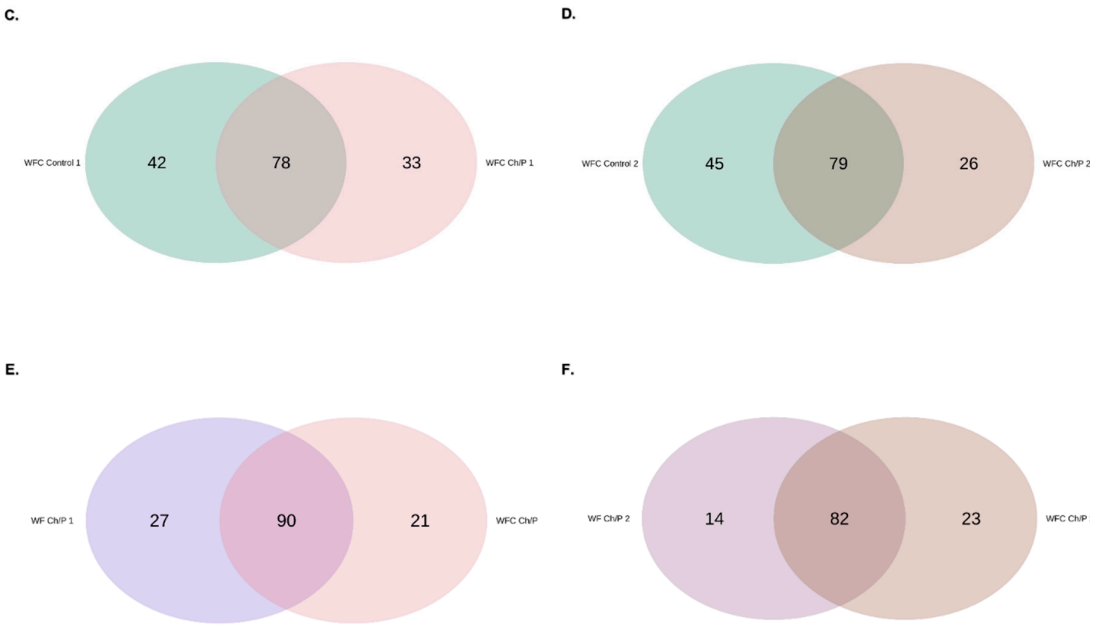

Figure 16. Venn diagrams prepared based on the sequencing of the 16S rRNA gene. The data shown in the diagram refer to site-specific unique ASVs and the core microbiome.

3.3. Physicochemical Analysis of Sludge Samples and Biogas Efficiency

The use of organic substrates of varying composition in waste biogas plants offers the opportunity to achieve high process yields, but also poses limitations related to the need for fermentation monitoring. This allows the process to be controlled and steered. During the decomposition of biomass, especially materials rich in fatty carbohydrates, there can be a rapid release of volatile fatty acids (VFAs) in the first stage, which often results in an acidified environment [36,38].

In the case of the experiment presented here, the process was stable, as indicated by the recorded values of the pH parameters, VFA concentration and VFA/TA ratio. Appropriate substrate ratios selected according to the standard [42], the results of previously performed studies [35,37,41] and the high buffer capacity of the sewage sludge as inoculum provided a guarantee for the successful implementation of the study [33–35]. pH values ranging from 6.9 to 7.6 were recorded, where a slight increase in pH occurred for mixtures with added cheese waste as a result of casein decomposition [36]. VFA concentration was obtained at relatively low values ranging from 1050 mg L^{-1} to 1970 mg L^{-1}, with higher values corresponding to samples with the cosubstrate system and with the addition of carrier. On the other hand, the VFA/TA ratio values were very similar, both for samples with and without carrier, and ranged from 0.26 to 0.43, confirming a stable process [64].

Quantitative changes in organic matter over time were also measured for in-process samples (from the four bioreactors studied) (see Figure 17). It was confirmed that during the fermentation of the mixtures studied, there was a loss of organic matter (with the release of biogas), which translated into a decrease in the content of volatile solids in the total solids of the fermented material.

 doi:10.20944/preprints202406.0813.v1

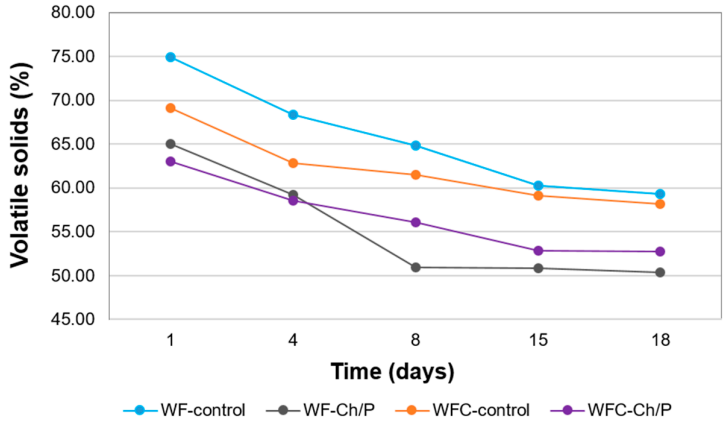

Figure 17. Changes in the content of volatile solids in samples collected during anaerobic digestion.

Due to the additional materials applied in the mixtures, a higher content of organic matter was observed in the control samples than in the samples with carrier addition. In the WF variant, a decrease in VS content of approx. 15% was observed, analogously in the control and test sample. In contrast, in the WFC variant, the same difference was approx. 11%, also for both samples. The amount of decomposed organic matter thus depended on the type of substrate rather than the presence of the carrier.

Using samples taken from the bioreactors tested, the rate of changes in organic matter content of the mixtures tested was also analysed (see Figure 18).

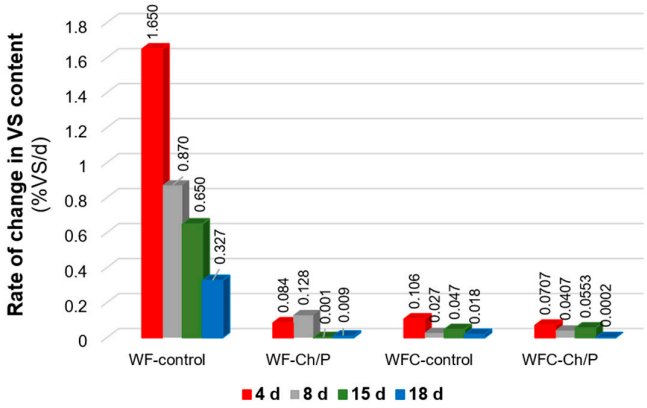

Figure 18. Rate of changes in the content of volatile solids in samples collected during anaerobic digestion.

It was found that this parameter was higher for the control samples than for the test samples, which could be related to the addition of carrier to the test samples. At the same time, a higher rate of change was found for the WF variant than for the WFC variant, which could be related to the type of substrate subjected to the fermentation process and is consistent with the greater decrease in VS content in the mixture shown earlier.

Qualitative changes, with respect to the chemical composition of the bioreactors, occurring during the process were investigated using the FT–IR infrared spectroscopy technique and the results obtained are shown in Figures 19a–d.

 doi:10.20944/preprints202406.0813.v1

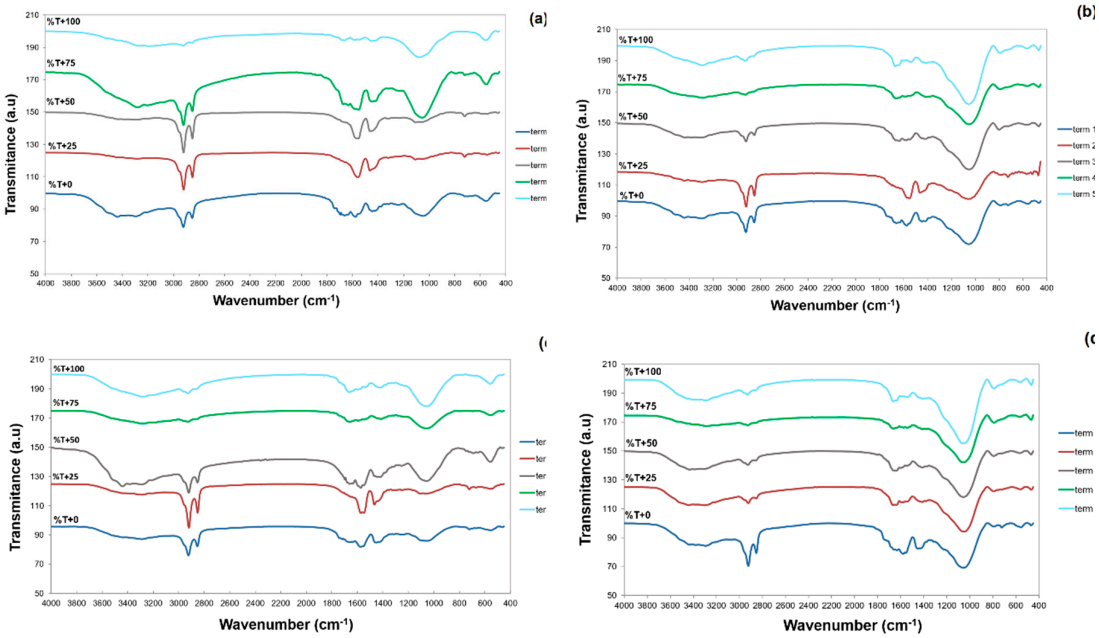

Figure 19. FT–IR spectra of samples collected during anaerobic digestion from batches:
(a) WF – control, (b) WF – Ch/P, (c) WFC – control, (d) WFC – Ch/P.

When interpreting the accompanying FT-IR spectra, it should be emphasised that the base material of the batches is stabilised sewage sludge (acting as an inoculum), hence the shape of the curves shows great similarity to the spectra of pure sewage sludge. It should also be emphasised that with such a small (yet consistent with the norm for the organic load of an anaerobic bioreactor) proportion of other organic materials (substrates), there could not have been overreaction of the materials. Hence, the spectral shape for all four samples is essentially identical. Differences occur in the size of the characteristic bands, which may indicate different kinetics of decomposition of the individual substances in the bioreactors. The rate of biodegradation may be influenced either by the proportion of carrier or, as inferred earlier (Figure 18), by the arrangement of the substrates undergoing the process. Both Grube et al., 2006 and Matheri et al., 2020 confirmed that the chemical composition of sewage sludge samples influences the shape of FT–IR spectra, which at the same time has an impact on the degradation process [65,66].

Sewage sludge contains mainly proteins, carbohydrates and lipids [67], however, the digested sludge of carbon compounds may contain considerably less. FT–IR spectra of sewage sludge presented in Figures 19a–d, showed a broad and intense band at 3200-3600 cm^{-1}, which was attributed to O–H and N–H stretching vibrations. These functional groups confirm the presence of alcohols, carboxylic acids and amides/amines, mainly derived from sewage sludge. The presence of a peak at about 3400 cm^{-1} in the dried samples analysed spectroscopically indicates the presence of alcohols, phenols, ethers and acids. This area in the samples exhibited comparable sizes, undergoing some flattening. On the other hand, two further bands appearing at around 2900 cm^{-1} and 2800 cm^{-1}, are particularly prominent at the first sampling dates, as two sharp peaks. These are attributed to asymmetric and symmetric C–H stretching vibrations, respectively, and their shrinkage (indicative of the decomposition of aliphatic chains in carbohydrates and lipids) is particularly observable in Figures 19b,d (samples with the addition of carriers), but least in the control sample with the addition of wafer waste alone. This phenomenon suggests a beneficial effect of combining both the carrier additive and the cosubstrate acting in synergy in the system [36]. In addition to fat and carbohydrates, which were derived from both inoculum (sludge) and substrates, protein was present in the samples, as indicated by the presence of amide I band and amide II band. These two bands, which gradually disappeared on the spectra of successive terms were recorded at 1650 cm^{-1} and 1546 cm^{-1}, (C=O stretching and N–H bending vibrations). C–O stretching vibrations between 1000 and 1200 cm^{-1}

 doi:10.20944/preprints202406.0813.v1

confirmed the presence of cellulose, which is a characteristic component of sewage sludge, as noted in their work by Yang et al., 2007 and Pilarska et al., 2019 [33,68]. In addition, small peaks of existence between 600 and 900 cm^{-1} representing aromatic compounds are observable. The presented characterisation of the spectra is consistent with the literature data [66,69]. The shape of the spectra, whose changes occurring during the process are particularly discernible with carbon-related functional groups, indicates the dependence of the degradation rate on both the presence of the carrier and the choice of cosubstrate, where, in the case analysed, the combination of confectionery and cheese waste as a balanced medium for the cells is of particular importance [36].

The biogas yield results obtained show a positive effect of both the addition of the carrier and the combination of confectionery and dairy waste in the cosubstrate system, which corresponds to the results of the analyses presented above (Figures 17–19). For the fermented sample of stand-alone wafer substrates (WF–control and WF–Ch/P), the addition of a cell carrier based on chitosan and perlite (3:1) contributed to a 12.05% increase in biogas/methane generation efficiency (Table 7). This addition, as an effective support for methanogenic cells, also resulted in an increase in the methane content of the biogas (from 53.2% to 55.5%), indicating an increase in the decomposition rate of organic matter. Combining the cosubstrate used in the system with porous and compatible microbial carriers, gives a definite improvement in process efficiency, as already proved by the results of a study by the same authors [36]. In the WFC–control and WFC–Ch/P systems, there was a 19.16% increase in process yield, which is very close to the results of studies with silica/lignin carrier (4:1) [37]. In comparison with other carriers previously tested by the same researchers, the values obtained are comparable or slightly lower [14,37]. These include a carrier such as diatomaceous earth/peat (3:1) or granulated PLA (which acted as both a carrier and a medium for the cells). Nevertheless, all, both currently discussed and presented in previous publications, carrier materials are worthy of consideration, due to their properties, favourable impact on process efficiency, affordability and price.

 doi:10.20944/preprints202406.0813.v1

Table 7. Total biogas and methane efficiency.

Samples	Biogas				Methane				CH_4	
	($m^3 Mg^{-1}$ TS)	MU (±)	($m^3 Mg^{-1}$VS)	MU (±)	($m^3 Mg^{-1}$TS)	MU (±)	($m^3 Mg^{-1}$VS)	MU (±)	(%)	MU (±)
WF–contr.	468.19	16.68	661.13	26.15	249.08	8.80	351.72	14.03	53.2	2.2
WF–Ch/P	524.61	18.69	740.08	29.30	291.16	10.28	411.14	16.40	55.5	2.3
WFC–contr.	545.21	19.42	780.42	30.86	333.12	11.76	476.84	19.02	61.1	2.5
WFC–Ch/P	565.18	20.13	798.27	31.57	366.80	12.95	518.08	20.67	64.9	2.7

MU – measurement uncertainty; contr. – control.

The volume of methane, obtained from the WF–control, in terms of volatile solids (VS) was 351.72 $m^3 Mg^{-1}$ VS (see Table 7) and increased to 411.14 $m^3 Mg^{-1}$ VS as a result of the addition of the carrier. The amount of methane obtained from the control cosubstrate sample was greater at 476.84 $m^3 Mg^{-1}$ VS. The addition of carrier to the WFC–Ch/P system increased the methane productivity, reaching 518.08 $m^3 Mg^{-1}$ VS.

4. Discussion

The development and use of microbial carriers in AD process offer significant prospects for enhancing the efficiency and stability of biogas production. These carriers, often referred to as bio-carriers or microbial carriers, provide a support structure for microbial communities, improving the anaerobic digestion process. In the AD process as a microbial carrier, in addition to the zeolites mentioned in the introduction [9–11], the following have also been tested: granulated polymeric support [poly(acrylonitrile-acrylamide)] [70], rubberised-coir [71], 'Magnetite+foam carrier' system [72], magnetite-modified zeolite [12], pumice [73], nanofibre membrane [74], and biochar [75]. In their study, Liu et al. (2017) focused exclusively on fibrous biofilm carriers, testing polypropylene, polyester, polyamide, and polyurethane fibre materials, with the most favorable results obtained from the application of polypropylene fibre [12]. On the other hand, recently, Zamrisham et al., 2024 conducted interesting research on integrating lava rock, red clay, and ceramic bio ring as support carriers in the anaerobic digestion of landfill leachate with liquidised food waste [76]. Research on carriers in the anaerobic digestion of organic waste of various origins is therefore conducted extensively, indicating their significant importance and tremendous potential of carrier materials. The authors of the present study have so far tested carrier systems of silica/lignin, diatomaceous earth/peat, and granular polylactide [17,37,44]. Pilarska et al. successfully selected materials that complement each other in terms of properties and functions performed in the process.

In the case of chitosan's participation in anaerobic digestion, which is the subject of research in this study, the increase in methane production can be attributed not only to its developed surface area but also to its specific chemical structure and the action of this material [21]. Yin and Chen 2022 proved the large effect of the contribution of chitosan (CTS) on the AD process of waste activated sludge (WAS) [24]. The results showed that the methane production potential of WAS was positively correlated with the CTS content. The presence of 30 g/kg of total suspension of CTS in the same study increased the cumulative methane production from 215 ± 1.52 to 272 ± 1.83 mL g^{-1} of volatile suspended solids. According to the cited researchers, the positively charged amino groups in chitosan

 doi:10.20944/preprints202406.0813.v1

neutralise the hydroxyl and carboxyl groups of extracellular polymeric substances, which reduces the negative charge of the sludge surface and promotes sludge agglomeration. Chitosan also slows down hydrolysis and reduces acidification by immobilizing hydrolase and acidulase enzymes, which has a stabilising effect on the course of anaerobic digestion. On the other hand, this additive flocculates humus to avoid its interference with electron transfer, thereby increasing the activity of coenzyme F420 and methanogenesis. Tetteh et al., 2022 also used chitosan in chitosan–magnetite (nCM; magnetite Fe_3O_4) and chitosan–titania–magnetite (nCTM) systems as biocatalysts for bioremediation of wastewater with methanogenic activity enhancement [26]. The authors concluded that nCTM is a very potent biocatalyst with biostimulatory effects on biogas production and methanogenic activity with a 75% degradation rate. Their study, on the other hand, showed that the development of nanobiocatalysts could provide a viable alternative to conventional anaerobic biogas production in wastewater treatment. In contrast, Nie et al., 2023 elucidated the mechanism of action of a chitosan-magnetite system, chitosan–Fe_3O_4 [25]. Sediment analysis showed that the chitosan–Fe_3O_4 material promoted the secretion of proteins and humic substances in extracellular polymeric substances and increased the electron transfer activity of the system by 71.4%. Microbiological community analysis showed that chitosan–Fe_3O_4 enriched the abundance of *Peptoclostridium* and *Methanosaeta* participated in direct interspecies electron transfer. Thus, the addition of the chitosan–Fe_3O_4 [25], as well as chitosan [24] or magnetite [26] itself, can promote a direct interspecies electron transfer pathway to maintain stable methanogenesis. Materials thus increase the abundance of methanogens, which naturally contributes to increased methane production [17]. Thus, the action of chitosan is multifunctional and takes place within different molecular pathways. From the point of view of improving the efficiency of biogas production, it is clear that continued AD research involving chitosan combined in defined substance systems is necessary.

With regard to perlite, many functional applications as a microbial carrier have been reported, particularly in the construction industry. Microbial mineralisation technology enables self-diagnosis. The direct incorporation of active microorganisms leads to an interaction between the microorganisms and the cement matrix, which has a positive effect on bacterial survival and the durability of the matrix itself [77]. However, the alkaline environment and the dense internal structure necessitate additional methods of bacterial protection, which are covered by a number of scientific studies [78]. For example, Jiang et al., 2020 investigated the effect of expanded perlite (EP) wrapped in various materials as a carrier for bacteria and nutrients to correct cracks and improve the ability of concrete to regenerate [79]. EP particles were found to improve the healing capacity of concrete cracks after the wrapping process. This effect was particularly noticeable when EP particles immobilised by bacterial spores were wrapped with a low-alkaline, potassium-magnesium phosphate-based material). This result was also confirmed in water permeability tests. On the other hand, a study by Yan et al., 2024 confirmed, among other things, that the number of microbial colonies decreases with decreasing freezing temperatures and that the smaller particle size of perlite, as a carrier, exacerbates the adsorption effect and, at the same time, the protective effect on microorganisms in alkaline environments [80]. With regard to the role of perlite as a microbial carrier in biogas production, it should be noted that this type of application of the material in question has so far been rare. However, as mentioned earlier, it has been proven that this application is possible. Moreover, it has significant effects in the form of increased immobilisation of microorganisms and accelerated substrate degradation, both under aerobic and anaerobic conditions [81].

As the above analysis confirms, research on carriers in AD of organic wastes of various origins is being conducted in large numbers, demonstrating their great importance and potential. The increased surface area of porous carriers facilitates the formation of biofilms in which microorganisms can aggregate and interact, enhancing their metabolic activity. This results in faster and more efficient decomposition of organic matter. Current advances in materials science have led to the development of a trend of combining materials into functional systems, involving natural materials (e.g., zeolite, biocarbon), synthetic polymers and nanomaterials. Each type of carrier offers unique properties that can be used in specific AD applications. Research is also currently underway to develop dedicated microbial consortia that can be immobilised on the carriers. These consortia are

 doi:10.20944/preprints202406.0813.v1

optimised to degrade specific types of feedstocks, increasing the overall efficiency and effectiveness of the AD process. It is also worth mentioning that the combination of microbial carriers with advanced monitoring and control systems offers a huge opportunity to optimise anaerobic digestion in real time. Sensors and automation can provide continuous feedback on microbial activity, enabling dynamic adjustments to operating conditions.

In summary, the prospects for the development and use of microbiological carriers (including systems such as the studied combination of chitosan and perlite) in anaerobic digestion are promising. By enhancing microbial activity, improving process stability and increasing methane yields, these materials can significantly increase the efficiency and sustainability of biogas production. Ongoing research, technological advances and successful pilot projects will be key to overcoming current challenges and realising the full potential of microbial carriers in anaerobic digestion.

5. Conclusions

The results of the analysis of the physico-chemical properties and the chitosan/perlite (3:1) carrier tested confirmed that this material system is a suitable proposal for use in anaerobic digestion. This carrier is characterised by a well-developed surface area, porosity, thermal stability, as well as being accessible and environmentally friendly. As shown by other analyses conducted as part of the experiment, this carrier induces targeted changes in the anaerobic biodegradation environment, with a modifying effect on the microbiome, ensuring increased participation during the process of Firmicutes, Synergistetes and Proteobacteria, which have an important influence on the degradation of substrates combined with sewage sludge. Analysis of removal kinetics of organic matter and FT–IR spectroscopy indicated a dependence of the degradation rate on both the combination of substrates used and the presence of a carrier. The values of the monitoring parameters confirmed a stable degradation process. These factors resulted in an increase in methane productivity: for WF–control by 12.05%, while for WFC–control, by 19.16%. The volume of methane for WF–control increased from 351.72 $m^3 Mg^{-1}$ VS to 411.14 $m^3 Mg^{-1}$ VS, while for the cosubstrate sample, it increased from 476.84 $m^3 Mg^{-1}$ VS to 518.08 $m^3 Mg^{-1}$ VS.

In order to understand the interactions between different types of microbial media and different microbial communities, further studies involving material systems with specific properties are required. Comprehensive studies support the optimisation of carrier design and microbial selection for specific AD applications.

Author Contributions: Conceptualisation, A.A.P.; methodology, A.A.P., A.M.-G. and M.M.; software, A.A.P., A.M.-G. and A.K.-W.; validation, K.P., M.M. and R.J.; formal analysis, A.A.P., T.K., K.P; investigation, A.A.P., A.M-G., M.M; and A.K.-W resources, A.A.P. and R.J.; data curation, A.A.P., A.M.-G., M.M. and K.P.; writing—original draft preparation, A.A.P.; writing—review and editing, A.A.P., A.M-G.; visualisation, A.A.P, A.M.-G.; supervision, T.K.; project administration, A.A.P.; funding acquisition, A.A.P. and T.K. All authors have read and agreed to the published version of the manuscript.

Funding:

Institutional Review Board Statement: Not applicable.

Informed Consent Statement: Not applicable.

Conflicts of Interest: The authors declare no conflict of interest.

References

1. Ajayi-Banji, A.; Rahman S. A review of process parameters influence in solid-state anaerobic digestion: Focus on performance stability thresholds. *Renew. Sustain. Energy Rev.* **2022**, *167*, 112756.
2. Assis, T.I.; Gonçalves, R.F. Valorization of food waste by anaerobic digestion: A bibliometric and systematic review focusing on optimization. *J. Environ. Manage.* **2022**, *320*, 115763.
3. Dompara, I.; Maragkaki, A.; Papastefanakis, N.; Floraki, C.; Vernardou, D.; Manios, T. Article effects of different materials on biogas production during anaerobic digestion of food waste. *Sustainability* **2023**, *15*, 5698.

 doi:10.20944/preprints202406.0813.v1

4. Yadav, M.; Joshi, C.; Paritosh, K.; Thakur, J.; Pareek, N.; Masakapalli, S.K.; Vivekanand, V. Reprint of Organic waste conversion through anaerobic digestion: A critical insight into the metabolic pathways and microbial interactions. *Metab. Eng.* **2022**, *17*, 62–76.
5. Zhou, M.; Yang, H.; Zheng, D.; Pu, X.; Liu, Y.; Wang, L.; Zhang, Y.; Deng, L. Methanogenic activity and microbial communities characteristics in dry and wet anaerobic digestion sludges from swine manure. *Biochem. Eng. J.* **2019**, *15*, 107390.
6. Júnior, A.D.N.F.; Etchebehere, C.; Zaiat, M. Mesophilic hydrogen production in acidogenic packed-bed reactors (APBR) using raw sugarcane vinasse as substrate: influence of support materials. *Anaerobe*. **2015**, *34*, 94–105.
7. Gong, W.J.; Liang, H.; Li, W.Z.; Wang, Z.Z. Selection and evaluation of biofilm carrier in anaerobic digestion treatment of cattle manure. *Energy* **2011**, *36*, 3572–3578.
8. Liu, Y.; Zhu, Y.; Jia, H.; Yong, X.; Zhang, L.; Zhou, J.; Cao, Z.; Kruse, A.; Wei, P. Effects of different biofilm carriers on biogas production during anaerobic digestion of corn straw. *Bioresour. Technol.* **2017**, *244*, 445–451.
9. Weiß, S.; Zankel, A.; Lebuhn, M.; Petrak, S.; Somitsch, W.; Guebitz, G.M. Investigation of microorganisms colonising activated zeolites during anaerobic biogas production from grass silage. *Bioresour. Technol.* **2011**, *102*, 4353–4359.
10. Montalvo, S.; Guerrero, L.; Borja, R.; Sánchez, E.; Milán, Z.; Cortés, I.; de la Rubia, M.A. Application of natural zeolites in anaerobic digestion processes: A review. *Appl. Clay Sci.* **2012**, *58*, 125–133.
11. Weiß, S.; M. Lebuhn, M.; Andrade, D.; A. Zankel, A.; Cardinale, M.; Birner-Gruenberger, R.; Somitsch, W.; Ueberbacher, B.J.; Guebitz, G.M. Activated zeolite– suitable carriers for microorganisms in anaerobic digestion processes? *Appl. Microbiol. Biotechnol.* **2013**, *97*, 3225–3238.
12. Jin, H.J.; Yao, X.Y.; Tang, C.C.; Zhou, A.J.; Liu, W.; Ren, Y.X.; Li, Z.; Wang, A.; He, Z.W. Magnetite modified zeolite as an alternative additive to promote methane production from anaerobic digestion of waste activated sludge. *Renew. Energy* **2024**, *224*, 120181.
13. Langxian, S.; Lintong, Z.; Xin, Y.; Maoyou, Y.; Jialin, L.; Minchun, H.; Xidan, F.; Lianhua, L. Dual roles in interspecies electron transfer of carbon-based materials for accelerating anaerobic digestion of food waste. *Biochem. Eng. J.* **2024**, *203*, 109182.
14. Pilarska, A.A.; Pilarski, K.; Adamski, M.; Zaborowicz, M.; Dorota Cais-Sokolińska, D.; Wolna-Maruwka, A.; Niewiadomska, A. Eco-friendly and effective diatomaceous earth/peat (DEP) microbial carriers in the anaerobic biodegradation of food waste products. *Energies* **2022**, *15*, 3442.
15. Cayetano, R.D.A.; Kim, G.B.; Park, J.; Yang, Y.H.; Jeon, B.C.; Jang, M.; Kim, S.H. Biofilm formation as a method of improved treatment during anaerobic digestion of organic matter for biogas recovery. *Bioresour. Technol.* **2022**, *344*, 126309.
16. Ouboter, H.T.; Mesman, R.; Sleutels, T.; Postma, J.; Wissink, M.; Jetten, M.S.M.; Heijne, A.T.; Berben, T.; Welte, C.U. Mechanisms of extracellular electron transfer in anaerobic methanotrophic archaea. *Nat. Commun*. **2024**, *15*, 1477.
17. Pilarska, A.A.; Wolna-Maruwka, A.; Niewiadomska, A.; Jarosław Grządziel, J.; Gałązka, A.; Paluch, E.; Borowiak, K.; Pilarski, K. Quantitative and qualitative changes in the genetic diversity of bacterial communities in anaerobic bioreactors with the diatomaceous earth/peat cell carrier. *Cells* **2022**, *11*, 2571.
18. Popa, A.; Visa, A.; Maranescu, B.; Hulka, I.; Lupa, L. Chemical modification of chitosan for removal of Pb(II) ions from aqueous solutions. *Materials* **2021**, *14*, 7894.
19. Satitsri, S.; Muanprasat, C. Chitin and chitosan derivatives as biomaterial resources for biological and biomedical applications. *Molecules* **2020**, *25*, 5961.
20. Stefanowska, K.; Woźniak, M.; Dobrucka, R.; Ratajczak, I. Chitosan with natural additives as a potential food packaging. *Materials* **2023**, *16*, 1579.
21. Fenice, M.; Gorrasi, S. Advances in chitin and chitosan science. *Molecules* **2021**, *26*, 1805.
22. Olajire, A.A.; Bamigbade, L.A. Green synthesis of chitosan-based iron@silver nanocomposite as adsorbent for wastewater treatment. *Water Res. Ind.* **2021**, 26, 100158.
23. Poureini, F.; Nikzad, M. *Application of Chitosan for wastewater treatment*. 2nd International Conference on Sustainable Development, Strategies and Challenges with a Focus on Agriculture, Natural Resources, Environment and Tourism, 23–25 Feb 2016, Tabriz, Iran.
24. Yin, M.; Chen, H. Unveiling the dual faces of chitosan in anaerobic digestion of waste activated sludge. *Bioresour. Technol*. **2022**, *344*, 126182.
25. Nie, W.; Lin, Y.; Wu, X.; Wu, S.; Li, X.; Cheng, J.J.; Yang, C. Chitosan–Fe_3O_4 composites enhance anaerobic digestion of liquor wastewater under acidic stress. *Bioresour. Technol*. **2023**, *377*, 128927.
26. Tetteh, E.K.; Amo-Duodu, G.; Rathilal, S. Biogas production from wastewater: Comparing biostimulation impact of magnetised–chitosan and –titania chitosan. *Mater. Today Proc.* **2022**, *62*, S85–S90.
27. Yilmazer, S.; Ozdeniz, M.B. The effect of moisture content on sound absorption of expanded perlite plates. *Build. Environ.* **2005**, *40*, 311–318.

28. Aksoy, Ö.; Alyamaç, E.; Mocan, M.; Sütçü, M.; Uçar, N.Ö.; Seydibeyoğlu, M.Ö. Characterization of perlite powders from Izmir, Türkiye region. *Physicochem. Probl. Miner. Process*. **2022**, *58*, 155277.
29. Yan, Y.; Jia, G.; Zhang, Y.; Gao, Y.; Li, Z. The influence of expanded perlite as a bio-carrier on the freeze–thaw properties of self-healing concreto. *Constr. Build. Mater.* **2023**, *409*, 133891.
30. Yan, Y.; Liu, W.; Jia, G.; Zhang, Y.; Gao, Y.; Li, Z. Application of expanded perlite immobilized microorganisms in cementitious materials. *J. Build. Eng*. **2023**, *76*, 106834.
31. Porras, C.M.; Rodríguez, J.L.P.; Martínez, J.L. An evaluation of clay minerals as support materials in anaerobic digesters. *Environ. Technol*. **1998**, *19*, 811–819.
32. Ivankovic, T.; Kontek, M.; Mihalic, V.; Ressler, A.; Jurisic, V. Perlite as a biocarrier for augmentation of biogas–producing reactors from olive (*Olea europaea*) waste *Appl. Sci.* **2022**, *12*, 8808.
33. Pilarska, A.A.; Pilarski, K.; Waliszewska, B.; Zborowska, M.; Witaszek, K.; Waliszewska, H.; Kolasiński, M.; Szwarc-Rzepka, K. Evaluation of bio-methane yields for high-energy organic waste and sewage sludge: A pilot-scale study for a wastewater treatment plant. *Environ. Eng. Manag. J.* **2019**, *18*, 2019–2030
34. Pilarska, A.A.; Pilarski, K.; Wolna-Maruwka, A. Cell immobilization on lignin–polyvinylpyrrolidone material used for anaerobic digestion of waste wafers and sewage sludge. *Environ. Eng. Sci*. **2019**, *36*, 478–490.
35. Pilarska, A.A. Anaerobic co-digestion of waste wafers from the confectionery production with sewage sludge. *Polish J. Environ. Stud.* **2018**, *27*, 237–245.
36. Pilarska, A.A.; Wolna-Maruwka, A.; Pilarski, K.; Janczak, D.; Przybył, K.; Gawrysiak-Witulska, M. The use of lignin as a microbial carrier in the co-digestion of cheese and wafer waste. *Polymers,* **2019**, *11*, 2073.
37. Pilarska, A.A.; Wolna-Maruwka, A.; Niewiadomska; Pilarski, K.; Adamski, M.; Grzyb, A.; Grządziel, J.; Gałązka, A. Silica/lignin carrier as a factor increasing the process performance and genetic diversity of microbial communities in laboratory-scale anaerobic digesters. *Energies* **2021**, *14*, 4429.
38. Pilarska, A.A.; Pilarski, K.; Wolna-Maruwka, A.; Boniecki, P.; Zaborowicz, M. Use of confectionery waste in biogas production by the anaerobic digestion process, *Molecules* **2019**, *24*, 37.
39. Pilarska, A.; Linda, I.; Wysokowski, M.; Paukszta, D.; Jesionowski, T. Synthesis of $Mg(OH)_2$ from a magnesium salt and NH_4OH with direct functionalisation with poly(ethylene glycols). *Physicochem. Probl. Miner. Process.* **2012**, *48*, 631–643.
40. Pilarska, A.A.; Wolna-Maruwka, A.; Pilarski, K. Kraft lignin grafted with polyvinylpyrrolidone as a novel microbial carrier in biogas production. *Energies* **2018**, *11*, 3246–3268.
41. Pilarska, A.A.; Bula, K.; Pilarski, K.; Adamski, M.; Wolna-Maruwka, A.; Tomasz Kałuza, T.; Magda, P.; Boniecki, P. Polylactide (PLA) as a cell carrier in mesophilic anaerobic digestion–A new strategy in the management of PLA. *Materials* **2022**, *15*, 8113.
42. Norm VDI 4630. Fermentation of Organic Materials Characterization of the Substrate, Sampling, Collection of Material Data, Fermentation Tests; German Engineers Club: Düsseldorf, Germany, 2006.
43. DIN Guideline 38 414-S8. Characterisation of the Substrate, Sampling, Collection of Material Data, Fermentation Tests; German Institute for Standardization: Berlin, Germany, 1985.
44. Pilarska, A.A.; Marzec-Grządziel, A.; Paluch, E.; Pilarski, K.; Wolna-Maruwka, A.; Kubiak, A.; Kałuża, T; Kulupa, T. Biofilm formation and genetic diversity of microbial communities in anaerobic batch reactor with polylactide (PLA) addition. *Int. J. Mol. Sci.* **2023**, *24*, 10042.
45. R Core Team. R: A *Language and Environment for Statistical Computing*; R Foundation for Statistical Computing: Vienna, Austria, 2016.
46. Callahan, B.J.; McMurdie, P.J.; Rosen, M.J.; Han, A.W.; Johnson, A.J.A.; Holmes, S.P. DADA2: High-resolution sample inference from Illumina amplicon data. *Nat. Methods* **2016**, *13*, 581–583.
47. Wright, E.S. RDP v16 Modified Training Set for 16S rRNA Classification. 2019. Available online: http://www2.decipher.codes/ Classification/TrainingSets/RDP_v16-mod_March2018.RData (accessed on 2 January 2019).
48. Murali, A.; Bhargava, A.; Wright, E.S. IDTAXA: A novel approach for accurate taxonomic classification of microbiome sequences. *Microbiome* **2018**, *6*, 140.
49. McMurdie, P.J.; Holmes, S. cPhyloseq: An R package for reproducible interactive analysis and graphics of microbiome census data. *PLoS ONE* **2013**, *8*, e61217.
50. Sweah, Z.J.; Malk, F.H.; Hussain, W.A. *Determination of the optical parameter from chitosan doping with nicotine* Cite as: AIP Conference Proceedings 2213, 020065 (2020); Published Online: 25 March 2020 https://doi.org/10.1063/5.0000090.
51. Khoshraftar, Z.; Masoumi, H.; Ghaemi, A. On the performance of perlite as a mineral adsorbent for heavy metals ions and dye removal from industrial wastewater: A review of the state of the art. *Case Stud. Chem. Environ. Eng*. **2023**, *8*, 100385.
52. Hasan, S.; Ghosh, T.K.; Boddu, V.M. Dispersion of *chitosan* on *perlite* for enhancement of copper(II) adsorption capacity. *J. Hazard. Mater.* **2008**, *152*, 826–837.
53. Farrokhi, Z.; Sadjadi, S.; Raouf, F.; Bahri-Laleh, N. Novel bio-based Pd/chitosan-perlite composite bead as an efficient catalyst for rapid decolorization of azo dye. *Inorg. Chem. Commun*. **2022**, *143*, 109734.

54. Swayampakula, K.; Boddu, V.M.; Abburi, K. Competitive adsorption of Cu (II), Co (II) and Ni (II) from their binary and tertiary aqueous solutions using chitosan-coated perlite beads as biosorbent. *J. Hazard. Mater*. **2009**, *170*, 680–689.
55. Demirçivi, P. Synthesis and characterization of Zr(IV) doped immobilized cross-linked chitosan/perlite composite for acid orange II adsorption. *Int. J. Biol. Macromol.* **2018**, *118*, 340–346.
56. Patil, S.B.; Sawant, K.K. Chitosan microspheres as a delivery system for nasal insufflation. Colloids Surf. B: Biointerfaces **2011**, *84*, 384–389.
57. Nguyen, T.V.; Nguyen, T.T.H.; Wang, S.L.; Vo, T.P.K.; Nguyen, A.D. Preparation of chitosan nanoparticles by TPP ionic gelation combined with spray drying, and the antibacterial activity of chitosan nanoparticles and a chitosan nanoparticle–amoxicillin complex. *Res. Chem. Intermed.* **2017**, *43*, 3527–3537
58. Vaezifar, S.; Razavi, S.; Golozar, M.A.; Karbasi, S.; Morshed, M.; Kamali, M. Effects of some parameters on particle size distribution of chitosan nanoparticles prepared by ionic gelation method. *J. Clust. Sci.* **2013**, *24*, 891–903
59. Reka, A.A.; Pavlovski, B.; Lisichkov, K.; Jashari, A.; Boev, B.; Boev, I.B.; Lazarova, M.; Eskizeybek, V.; Oral, A.; Jovanovski, G.; Makreski, P. Chemical, mineralogical and structural features of native and expanded perlite from Macedonia. *Geol. Croat.* **2019**, *72*, 215–221.
60. Dhawade, P.P.; Jagtap, R.N. Characterization of the glass transition temperature of chitosan and its oligomers by temperature modulated differential scanning calorimetry. *Adv. Appl. Sci. Res.* **2012**, *3*, 1372–1382.
61. Acosta-Ferreira, S.; Castillo, O.S.; Madera-Santana, J.T.; Mendoza-García, D.A.; Núñez-Colín, C.A.; Grijalva-Verdugo, C.; Villa-Lerma, A.G.; Morales-Vargasa, A.T.; Rodríguez-Núñeza, J.R. Production and physicochemical characterization of chitosan for the harvesting of wild microalgae consortia. *Biotechnol. Rep.* **2020**, *28*, e00554.
62. Karaipekli, A.; Biçer, A.; Sarı, A.; Tyagi, V.V. Thermal characteristics of expanded perlite/paraffin composite phase change material with enhanced thermal conductivity using carbon nanotubes. *Energy Conv. Manage.* **2017**, *134*, 373–381
63. Major, N.; Sørensen, S.J.S.J.; Ban, D.; Nesme, J.; Grosch, R.; Ban, S.G.; Schikora, A.; Cerne, M.; Schierstaedt, J. Influence of sewage sludge stabilization method on microbial community and the abundance of antibiotic resistance genes. *Waste Manage.* **2022**, *154*, 126–135.
64. Chen,Y.; Cheng, J.J.; Creamer, K.S. Inhibition of anaerobic digestion process: A review. *Bioresour. Technol.* **2008**, *99*, 4044–4064
65. Grube, M.; Lin, J.; Lee, P.H.; Kokorevicha, S. Evaluation of sewage sludge-based compost by FT-IR 590 spectroscopy. *Geoderma* **2006**, *130*, 324-333.
66. Matheri, A.N.; Eloko, N.S.; Ntuli, F.; Ngila, J.C. Influence of pyrolyzed sludge use as an adsorbent in removal of selected trace metals from wastewater treatment. *Case Stud. Chem. Environ. Eng.* **2020**, *2*, 100018.
67. Pilarska, A.A.; Pilarski, K.; Witaszek, K.; Waliszewska, H.; Zborowska, M.; Waliszewska, B.; Kolasi'nski, M.; Szwarc-Rzepka, K. Treatment of dairy waste by anaerobic digestion with sewage sludge. *Ecol. Chem. Eng.* **2016**, *23*, 99–115.
68. Yang, H., Yan, R., Chen, H., Lee, D.H., Zheng, C. Characteristics of hemicellulose, cellulose and lignin pyrolysis. *Fuel* **2007**, *86*, 1781–1788.
69. Hantoko, D.; Kanchanatip, A.E.; Yan, M.; Weng, Z.; Gao, Z.; Zhong, Y. Assessment of sewage sludge gasification in supercritical water for H_2-rich syngas production. *Process Saf. Environ. Prot.* **2019**, *131*, 63–72.
70. Lalov, I.G.; Krysteva, M.A.; Phelouzat, J.L. Im provement of biogas production from vinasse via covalently immobilized methanogens. *Bioresour. Technol.* **2001**, *79*, 83.
71. Dhaked, R.K.; Ramana, K.V.; Tomar, A.; Waghmare, C.; Kamboj, D.V.; Singh, L. Immobilization of anaerobic bacteria on rubberized-coir for psychrophilic digestion of night soil. *Anaerobe* **2005**, *11*, 217–224.
72. Yang, Z.; Sun, H.; Kurbonova, M.; Zhou, L.; Arhin, S.G.; Papadakis, V.G.; Goula, M.A.; Liu, G.; Zhang, Y.; Wang, W. Simultaneous supplementation of magnetite and polyurethane foam carrier can reach a Pareto–optimal point to alleviate ammonia inhibition during anaerobic digestion. *Renew. Energy* **2022**, *189*, 104–116.
73. Zhang, Y.; Hu, Q.; Wang, T.; Jin, Z.; Luo, T.; Huang, J.; Xu, G.; Zhan, Y.; Wang, H. Pumice as biological carriers improve impact load resistance of UASB reactors during the treatment of raw incineration leachates. *Pol. J. Environ. Stud.* 2022, *31*, 1975– 1983.
74. Liu, Y.; Xi, Y.; Ye, X.; Zhang, Y.; Wang, C.; Jia, Z.; Cao, C.; Han, T.; Du, J.; Kong, X.; Chen, Z. Composite nanofiber membranes to enhance the performance of high solids anaerobic digestion of organic rural household waste resources. *Renew. Energy* **2024**, *220*, 119564.
75. Zhao, W.; Hu, T.; Ma, H.; Li, D.; Zhao, Q.; Jiang, J.; Wei, L. A review of microbial responses to biochar addition in anaerobic digestion system: Community, cellular and genetic level findings. *Bioresour. Technol.* **2024**, *391*, 129929.

 doi:10.20944/preprints202406.0813.v1

76. Razak, N.A.F.Z.M.S.A.; Jaman, S.I.K.J.; Harun, M.R. Biogas production by integrating lava rock, red clay & ceramic bio ring as support carrier in treatment of landfill leachate with liquidised food waste. *Biochem. Eng. J.* **2024**, *204*, 109221.
77. Yan, Y.; Jia, G.; Zhang, Y.; Gao, Y.; Li, Z. The influence of expanded perlite as a bio-carrier on the freeze–thaw properties of self-healing concreto. *Constr. Build. Mater*. **2023**, *409*, 133891.
78. Yan, Y.; Liu, W.; Jia, G.; Zhang, Y.; Gao, Y.; Li, Z. Application of expanded perlite immobilized microorganisms in cementitious materials. *J. Build. Eng*. **2023**, *76*, 106834.
79. Jiang, L.; Jia, G.; Jianga, C.; Li, Z. Sugar-coated expanded perlite as a bacterial carrier for crack-healing concrete applications. *Constr. Build. Mater.* **2020**, *232*, 117222.
80. Yan, Y.; Liu, W.; Li, Z.; Jia, G.; Zhang, Y.; Ma, G.; Gao Y. Mechanical properties and frost resistance of self-healing concrete based on expanded perlite with different particle sizes as microbial carrier. *Constr. Build. Mater.* **2024**, *422*, 135450.
81. Ivankovic, Y.; Kontek, M.; Mihalic, V.; Ressler, A.; Jurisic, V. Perlite as a biocarrier for augmentation of biogas – Producing reactors from olive (*Olea europaea*) waste. *Appl. Sci.* **2022**, *12*, 8808.